Ab initio method for examining the halo structure of ^{6}He. I. Coordinate space two-nucleon correlations

Mengyao Huang,[1,2] Tobias Frederico,[3] Pieter Maris,[1] Peng Yin,[4,1]
Robert Basili,[1,5] Mark A. Caprio,[6] Patrick J. Fasano,[6,1] and James P. Vary[1]

[1]*Department of Physics and Astronomy, Iowa State University, Ames, Iowa 50011, USA*
[2]*Lawrence Livermore National Laboratory, P.O. Box 808, L-414, Livermore, California 94551, USA*
[3]*Instituto Tecnológico de Aeronáutica, DCTA, 12228-900 São José dos Campos, Brazil*
[4]*CAS Key Laboratory of High Precision Nuclear Spectroscopy, Institute of Modern Physics, Chinese Academy of Sciences, Lanzhou 730000, China*
[5]*Department of Mathematics, Iowa State University, Ames, Iowa 50011, USA*
[6]*Department of Physics and Astronomy, University of Notre Dame, Notre Dame, Indiana 46556, USA*

We evaluate pairwise correlations using full ground state wave functions for ^{4}He and ^{6}He obtained by *ab initio* configuration interaction methods with the Daejeon16 nucleon-nucleon interaction, to characterize the structures of these two systems. We show that the two-nucleon spatial correlations $f(r^n)$, for instance, the pair-identity operator r^0 and the square-separation operator r^2, can shed light on the halo structure of ^{6}He relative to ^{4}He. To the best of our knowledge, this is the first attempt of examining the nuclear structure directly using two-body spatial correlations projecting on two-body total quantum numbers (such as the two-body total spin S) with the no-core shell model (NCSM). Connecting the expectation values of r^0 for ^{6}He with those for ^{4}He, we conclude that the two valence neutrons in ^{6}He dominantly form a spin-singlet configuration when the symmetry regarding the probability of forming an arbitrary two-body total spin is respected. The root-mean-square separation between two nucleons for each projecting sector is calculated using the expectation value of r^2 combined with r^0. For completeness, even without fully convergent results, we compare the point-nucleon root-mean-square radii calculated from r^2 with those obtained from experiments.

I. INTRODUCTION

Clustering phenomena in atomic nuclei reflect both the degrees of freedom of individual nucleons and collective structures within the nucleus. As a natural example, certain nuclei near the "drip lines" (where nucleons are nearly free to escape) form a more tightly bound core and a "halo" made of one or more nucleons loosely bound to the core [1–5].

Neutron halos have drawn significant attention since the 1980s when the surprisingly large interaction cross section of ^{11}Li compared with other Li isotopes was observed in radioactive ion beam (RIB) transmission experiments [6–8]. They also display a narrow core momentum distribution in peripheral breakup reactions [9, 10]. Strong electric dipole ($E1$) excitations at low excitation energies were observed in some of the halo nuclei, attributed to their weakly bound halo neutron(s) undergoing excitation to the continuum states [11–13]. Although there is no clear-cut distinction between the halo and non-halo nuclei, halo nuclei are recognized by their shared characteristics. Nuclei with a neutron halo, for example, display a long tail in the neutron density distribution profile, and have small neutron separation energies for the halo neutron(s).

Over the years, many efforts have been made to extract the clustering information from *ab initio* calculations. The *ab initio* NCSM/RGM (no-core shell model/resonating group method) was used to perform calculations on a ^{4}He (g.s.) + n + n cluster basis which was consistent with *ab initio* NCSM calculations without a cluster basis [14–16]. Cluster form factors were extracted [17], and further improvements have been made to the work on three-cluster dynamics within the *ab initio* NCSM with continuum [16, 18]. The *ab initio* lattice approach implementing chiral effective field theory successfully modeled a 3-α structure for the Hoyle state of ^{12}C [19]. More recently, *ab initio* configuration interaction methods have revealed important roles of α-clustering in light nuclei including details on the ground and Hoyle excited state of ^{12}C [20]. In addition, measures of entanglement of ^{4}He and ^{6}He nuclei were explored using *ab initio* nuclear many-body calculations [21], where a core-valence structure naturally emerges from the full no-core calculation of ^{6}He by analyzing common features of entanglement.

From a computational point of view, studying the clustering properties of nuclei could help us design improved basis functions and to usefully subdivide the Hilbert space into regions of greater and lesser importance. Spatial information such as the average relative separations of nucleons in a system is key to characterizing the cluster wave functions.

Thus, we examine the structure of a nucleus by *ab initio* calculations, utilizing two-body correlations. Previously, one-body probabilities have been used in the *ab initio* NCSM [22] with great success in revealing information on the clustering of Li isotopes [23, 24] and ^{9}Be [24], a one-neutron halo nucleus. Using two-body operators has the advantage of unfolding the detailed structure of the dominant configuration and displaying the differences in the nucleon-nucleon correlations among pairs of nucleons in specific two-body states.

We choose ^{6}He as a test case for this new method ow-

ing to its relative simplicity. It is the lightest Borromean halo nucleus which means that none of the available two-component substructures (n-n or n-α in the α+n+n system) are bound when one removes any third component. In this case, the one-body density profile cannot fully reveal the geometrical structure for the $2n$-halo, while two-body correlations can probe the relative distance between the two valence neutrons compared with the relative distances of the other pairs of nucleons. Our primary focus is to introduce our method and demonstrate its application to ^{6}He in advance of achieving fully converged *ab initio* NCSM results for the two-body correlations that we develop and employ. We defer the development of suitable extrapolation methods for these two-body correlations to a later project.

In the following sections, we first introduce the coordinate space two-body operators we will use (Sec. II) and the approach to solving the quantum many-body problem (Sec. III). We then present and discuss the calculated expectation values of these two-body operators and how they relate to the halo structure of ^{6}He (Sec. IV).

II. CONSTRUCTING TWO-BODY OPERATORS IN COUPLED-J BASIS

In order to carry out a quantitative analysis of the distributions of nucleons and pairs of nucleons within a nucleus, one needs appropriate operators that sample these quantities. For this purpose, we will define one-body and two-body operators whose expectation values within the nuclear ground state will inform our detailed analysis of how nucleons are arranged in coordinate space on average. From this arrangement, we hope to infer if a halo structure is emerging from the quantum many-body wave functions.

A. One- and two-body operators in the occupation representation

One-body operators are defined as [25]

$$\mathcal{O}_{\rm 1B} = \sum_{\alpha,\beta} O_{\alpha\beta} a^\dagger_\alpha a_\beta, \tag{1}$$

where

$$O_{\alpha\beta} = \langle\alpha|\mathcal{O}|\beta\rangle \tag{2}$$

are the one-body matrix elements and the Greek subscripts label the single-particle states in an ordered sequence. The single-particle states are related to creation operators acting on the vacuum,

$$|\alpha\rangle = a^\dagger_\alpha|0\rangle. \tag{3}$$

Similarly, two-body operators are defined as [25]

$$\mathcal{O}_{\rm 2B} = \sum_{\alpha<\beta,\gamma<\delta} O_{\alpha\beta\gamma\delta} a^\dagger_\alpha a^\dagger_\beta a_\delta a_\gamma, \tag{4}$$

where

$$O_{\alpha\beta\gamma\delta} = \langle\alpha\beta|\mathcal{O}|\gamma\delta\rangle = \langle 0|a_\beta a_\alpha \mathcal{O} a^\dagger_\gamma a^\dagger_\delta|0\rangle \tag{5}$$

are the two-body matrix elements. Due to the fermion anticommutation relation $a^\dagger_\alpha a^\dagger_\beta = -a^\dagger_\beta a^\dagger_\alpha$, the two-body matrix elements are antisymmetric under interchange of each pair of two-body state labels.

Let us now focus only on the two-body operators. The expectation value of a two-body operator between an initial state $|\Phi_A\rangle$ and a final state $|\Phi'_A\rangle$ in a system of nucleons is thus

$$\langle\Phi'_A|\mathcal{O}_{\rm 2B}|\Phi_A\rangle = \sum_{\alpha\beta\gamma\delta} \rho_{\alpha\beta\gamma\delta}\ \langle\alpha\beta|\mathcal{O}|\gamma\delta\rangle, \tag{6}$$

where $\alpha<\beta, \gamma<\delta$ is implicitly assumed wherever summing pairs of two-body state labels, and

$$\rho_{\alpha\beta\gamma\delta} = \langle\Phi'_A|a^\dagger_\alpha a^\dagger_\beta a_\delta a_\gamma|\Phi_A\rangle \tag{7}$$

defines matrix elements of the two-body density matrix.

B. Two-body operators in the coupled-J basis

The standard basis we use is the single particle basis, which is denoted by its quantum numbers including radial quantum number n, orbital angular momentum l, spin s, total angular momentum j, total angular momentum projection m_j, isospin t and isospin projection t_z. We can use the short-hand notation

$$\alpha = \{n_\alpha, l_\alpha, \frac{1}{2}, j_\alpha, m_{j_\alpha}, \frac{1}{2}, t_{z\alpha}\}, \tag{8}$$

where the first "1/2" is for nucleon spin s and the second "1/2" is for nucleon isospin t.

To compute matrix elements of two-body operators in a basis with "good" angular momentum, two-body total angular momentum J, we work in terms of the spherical tensor coupled product [26], e.g.,

$$\{a^\dagger_\alpha a^\dagger_\beta\}_{J,M} = \sum_{m_{j_\alpha}, m_{j_\beta}} C^{\ j_\alpha\ \ j_\beta\ \ J}_{m_{j_\alpha} m_{j_\beta} M}\ a^\dagger_\alpha a^\dagger_\beta, \tag{9}$$

where M is the z-projection of the two-body total angular momentum. $C^{\ j_\alpha\ \ j_\beta\ \ J}_{m_{j_\alpha} m_{j_\beta} M}$ are the Clebsch-Gordan coefficients. The transformed coupled basis is called coupled-J basis. The resulting coupled-J basis states are

$$|\alpha\beta; J\rangle = \{a^\dagger_\alpha a^\dagger_\beta\}_J|0\rangle. \tag{10}$$

When one aims to calculate only observables represented by one-body and two-body operators, one may simply compute the one-body and two-body density matrices between the desired initial and final states, and the matrix elements of all one-body and two-body operators may subsequently be extracted from the weighted sum of these density matrices.

The two-body density matrix in the coupled-J basis, suppressing M for compactness of notation, is

$$\rho_{\{\alpha\beta\}_{J'}\{\gamma\delta\}_J} = \langle\Phi'_A|\{a^\dagger_\alpha a^\dagger_\beta\}_{J'}\{a_\delta a_\gamma\}_J|\Phi_A\rangle = \sum_{m_{j_\alpha},m_{j_\beta}} C^{j_\alpha\ j_\beta\ J'}_{m_{j_\alpha}\,m_{j_\beta}\,M'} \sum_{m_{j_\gamma},m_{j_\delta}} C^{j_\gamma\ j_\delta\ J}_{m_{j_\gamma}\,m_{j_\delta}\,M}\ \rho_{\alpha\beta\gamma\delta}\ . \tag{11}$$

The expectation value of a two-body operator in a system of nucleons expressed in the coupled-J basis can thus be written as

$$\langle\Phi_{A'}|\mathcal{O}_{\rm 2B}|\Phi_A\rangle = \sum_{\{\alpha\beta\}_{J'}\{\gamma\delta\}_J} \rho_{\{\alpha\beta\}_{J'}\{\gamma\delta\}_J}\ \langle\alpha\beta;J'|\mathcal{O}|\gamma\delta;J\rangle, \tag{12}$$

where $\mathcal{O}$ is redefined as an operator acting on the coupled-J basis.

C. Rotationally invariant operator with given two-body total spin and given pair of isospin projections

We consider matrix elements of local two-body operators of the form $O(r)P_S$, that is, a rotationally invariant (scalar) operator depending only on the relative spatial coordinate r of the two nucleons, in combination with the two-body total spin projection operator P_S, where $\langle S_1|P_S|S_2\rangle = \delta_{SS_1}\delta_{SS_2}$. We adopt the shorthand $\mathcal{O}(r)[S] \equiv O(r)P_S$, and below we will focus on operators $\mathcal{O}(r)[S,t_{za},t_{zb}]$ which also project on given isospin projections t_{za} and t_{zb} of the two nucleons.

Since the $O(r)$ operator is a rank-0 tensor, from the Wigner-Eckart theorem, $\langle\alpha\beta;J'M'|O(r)|\gamma\delta;JM\rangle = \delta_{J'J}\delta_{M'M}\langle\alpha\beta;J||O(r)||\gamma\delta;J\rangle$, where, in our convention, the double-bar (reduced) matrix element does not factor out $(2J+1)^{-\frac{1}{2}}$ and remains consistent with the Wigner-Eckart theorem formulated in Eq. (4.15) of Ref. [27].

In order to select the states of given two-body total spin, one can resolve quantities in terms of two-body total spin S ($\vec{S} = \vec{s}_\alpha + \vec{s}_\beta$) and two-body total orbital angular momentum L ($\vec{L} = \vec{l}_\alpha + \vec{l}_\beta$) by inserting

$$\mathbb{1} = \sum_{LS} |n_\alpha l_\alpha n_\beta l_\beta L, \tfrac{1}{2}\tfrac{1}{2}S;J\rangle\langle n_\alpha l_\alpha n_\beta l_\beta L, \tfrac{1}{2}\tfrac{1}{2}S;J| \tag{13}$$

twice, where the spin quantum numbers ($\frac{1}{2}$) are explicit while the isospin quantum numbers are omitted for simplification of the notation.

We find that the reduced matrix element of $\mathcal{O}(r)[S]$ can be expressed as

$$\begin{aligned}
&\langle\alpha\beta;J||\mathcal{O}(r)[S]||\gamma\delta;J\rangle \\
&= \sum_{L_1L_2S_1S_2} \langle\alpha\beta;J|n_\alpha l_\alpha n_\beta l_\beta L_1,\tfrac{1}{2}\tfrac{1}{2}S_1;J\rangle\langle n_\alpha l_\alpha n_\beta l_\beta L_1,\tfrac{1}{2}\tfrac{1}{2}S_1;J||O(r)||n_\gamma l_\gamma n_\delta l_\delta L_2,\tfrac{1}{2}\tfrac{1}{2}S_2;J\rangle\langle n_\gamma l_\gamma n_\delta l_\delta L_2,\tfrac{1}{2}\tfrac{1}{2}S_2;J|\gamma\delta;J\rangle \\
&\quad\times\delta_{SS_1}\delta_{S_1S_2} \\
&= \sum_L \langle n_\alpha l_\alpha n_\beta l_\beta L||O(r)||n_\gamma l_\gamma n_\delta l_\delta L\rangle\langle\alpha\beta;J|n_\alpha l_\alpha n_\beta l_\beta L,\tfrac{1}{2}\tfrac{1}{2}S;J\rangle\langle n_\gamma l_\gamma n_\delta l_\delta L,\tfrac{1}{2}\tfrac{1}{2}S;J|\gamma\delta;J\rangle,
\end{aligned} \tag{14}$$

where in the last line we have used the fact that $O(r)$ is rotationally invariant so the two-body total orbital angular momentum is invariant upon the action of $O(r)$, i.e. $\langle L_1|O(r)|L_2\rangle = \langle L_1|O(r)\delta_{L_1L_2}|L_2\rangle$. And we now drop the subscript of L for notational simplicity. There is no need to label J values in the reduced matrix elements, because $O(r)$ only produces a dependence on the radial and orbital quantum numbers.

We identify the "$LS-jj$" coupling coefficient [26, 28], i.e., the transformation coefficient between Russell-Saunders coupling and the spin-orbit coupling in Eq. (14) by first expanding the notation

$$\begin{aligned}
&\langle\alpha\beta;J|n_\alpha l_\alpha n_\beta l_\beta L,\tfrac{1}{2}\tfrac{1}{2}S;J\rangle \\
&= \langle n_\alpha l_\alpha \tfrac{1}{2} j_\alpha, n_\beta l_\beta \tfrac{1}{2} j_\beta;J|n_\alpha l_\alpha n_\beta l_\beta L,\tfrac{1}{2}\tfrac{1}{2}S;J\rangle \\
&= \langle l_\alpha \tfrac{1}{2} j_\alpha, l_\beta \tfrac{1}{2} j_\beta;J|l_\alpha l_\beta L,\tfrac{1}{2}\tfrac{1}{2}S;J\rangle \\
&= \sqrt{(2j_\alpha+1)(2j_\beta+1)(2L+1)(2S+1)} \begin{Bmatrix} l_\alpha & l_\beta & L \\ 1/2 & 1/2 & S \\ j_\alpha & j_\beta & J \end{Bmatrix},
\end{aligned} \tag{15}$$

where the curly brackets represent the $9j$ symbols, which is another way to write an assembly of Clebsch-Gordan coefficients.

One then obtains

$$\langle\alpha\beta;J||\mathcal{O}(r)[S]||\gamma\delta;J\rangle = \langle n_\alpha l_\alpha n_\beta l_\beta L||O(r)||n_\gamma l_\gamma n_\delta l_\delta L\rangle \times (2S+1)\sqrt{(2j_\alpha+1)(2j_\beta+1)(2j_\gamma+1)(2j_\delta+1)}\sum_L(2L+1)\begin{Bmatrix} l_\alpha & l_\beta & L\\ 1/2 & 1/2 & S\\ j_\alpha & j_\beta & J\end{Bmatrix}\begin{Bmatrix} l_\gamma & l_\delta & L\\ 1/2 & 1/2 & S\\ j_\gamma & j_\delta & J\end{Bmatrix}. \tag{16}$$

To apply this operator on a fixed pair of isospin z-projection values for two nucleons, we define $\mathcal{O}(r)[S,t_{za},t_{zb}] = O(r)P_SP_{t_{za},t_{zb}}$, with

$$\begin{aligned}\langle\alpha\beta;J||\mathcal{O}(r)[S,t_{za},t_{zb}]||\gamma\delta;J\rangle =& \langle\alpha\beta;J||\mathcal{O}(r)[S,t_{za},t_{zb}]\delta_{t_{z\alpha},t_{z\gamma}}\delta_{t_{z\beta},t_{z\delta}}||\gamma\delta;J\rangle\\ =& \langle\alpha\beta;J||\mathcal{O}(r)[S]||\gamma\delta;J\rangle\delta_{t_{z\alpha},t_{z\gamma}}\delta_{t_{z\beta},t_{z\delta}}[\delta_{t_{z\alpha},t_{za}}\delta_{t_{z\beta},t_{zb}}+(1-\delta_{t_{za},t_{zb}})\delta_{t_{z\alpha},t_{zb}}\delta_{t_{z\beta},t_{za}}],\end{aligned} \tag{17}$$

where the factor $(1-\delta_{t_{za},t_{zb}})$ preserves the normalization when $t_{za}=t_{zb}$.

The resulting matrix element becomes

$$\begin{aligned}\langle\alpha\beta;J'M'|\mathcal{O}(r)[S,t_{za},t_{zb}]|\gamma\delta;JM\rangle =& [\delta_{t_{z\alpha},t_{za}}\delta_{t_{z\beta},t_{zb}}+(1-\delta_{t_{za},t_{zb}})\delta_{t_{z\alpha},t_{zb}}\delta_{t_{z\beta},t_{za}}]\delta_{t_{z\alpha},t_{z\gamma}}\delta_{t_{z\beta},t_{z\delta}}\delta_{J'J}\delta_{M'M}\\ &\times(2S+1)\sqrt{(2j_\alpha+1)(2j_\beta+1)(2j_\gamma+1)(2j_\delta+1)}\\ &\times\sum_L(2L+1)\begin{Bmatrix} l_\alpha & l_\beta & L\\ 1/2 & 1/2 & S\\ j_\alpha & j_\beta & J\end{Bmatrix}\begin{Bmatrix} l_\gamma & l_\delta & L\\ 1/2 & 1/2 & S\\ j_\gamma & j_\delta & J\end{Bmatrix}\langle n_\alpha l_\alpha n_\beta l_\beta L||O(r)||n_\gamma l_\gamma n_\delta l_\delta L\rangle.\end{aligned} \tag{18}$$

We then introduce a notation to describe an operator acting within a system of nucleons, similar to the $U[u]$ and $V[v]$ operators defined in Ref. [29]. The subscript A of a two-body operator means to apply the operator on all nucleon pairs in the A-body space, $(\mathcal{O}_{2B})_A \equiv \sum_{i<j}^A \mathcal{O}_{2B}$. Similarly, the subscript A of a one-body operator means to apply the operator on all A nucleons, $(\mathcal{O}_{1B})_A \equiv \sum_i^A \mathcal{O}_{1B}$. Thus, the expectation value of $\mathcal{O}(r)_A[S,t_{za},t_{zb}]$ is

$$\begin{aligned}\langle\mathcal{O}(r)_A[S,t_{za},t_{zb}])\rangle &= \langle\sum_{i<j}^A\mathcal{O}(r_{ij})[S,t_{za},t_{zb}]\rangle\\ &= \sum_{\text{all q\#}}\sum_{i<j}^A{}_{ij}\langle\alpha\beta;J'M'|\mathcal{O}(r)[S,t_{za},t_{zb}]|\gamma\delta;JM\rangle_{ij},\end{aligned} \tag{19}$$

where $r_{ij} = |\vec{r}_i - \vec{r}_j|$ is the relative distance between the ith and jth nucleon, and $i,j = 1,2,\cdots A$. α and γ (β and δ) denote the initial and final single particle states of the ith (jth) nucleon, respectively. The overall summation runs over all quantum numbers ("all q#"). In the following, the subscript A is conveniently omitted when referring to the expectation values of the operator (denoted by a bracket directly around the operator), i.e., $\langle\mathcal{O}\rangle \equiv \langle\mathcal{O}_A\rangle$.

In Sec. II D and Sec. II E, we will define the pair-identity operator and the square-separation operator in given S and isospin projection pair (proton-proton, neutron-proton and neutron-neutron, indicated as pp, pn, and nn) sectors. Combining them will give us the information on mean square separations of a pp, pn or nn pair of nucleons with a given two-body total spin S, which will be illustrated in Sec. IV B.

D. Pair-identity operator

The pair-identity operator r^0 for a given two-body total spin S and a fixed pair of isospin projections is $\mathcal{O}(r)[S,t_{za},t_{zb}] = r^0[S,t_{za},t_{zb}] \equiv \mathbb{1}P_SP_{t_{za},t_{zb}}$, where the identity is the same as in Eq. (13). Applying this operator to the A-nucleon space, the expectation value

$$\langle r^0[S,t_{za},t_{zb}]\rangle = \sum_{\text{all q\#}}\sum_{i<j}^A{}_{ij}\langle\alpha\beta;J|P_SP_{t_{za},t_{zb}}|\gamma\delta;J\rangle_{ij}. \tag{20}$$

Summing over S in Eq. (20),

$$\begin{aligned}\langle r^0[t_{za},t_{zb}]\rangle =& \sum_{i<j}^A\sum_{\text{all q\#}}{}_{ij}\langle\alpha\beta;J|\mathbb{1}|\gamma\delta;J\rangle_{ij}\delta_{t_{z\alpha},t_{z\gamma}}\\ &\times\delta_{t_{z\beta},t_{z\delta}}[\delta_{t_{z\alpha},t_{za}}\delta_{t_{z\beta},t_{zb}}+(1-\delta_{t_{za},t_{zb}})\delta_{t_{z\alpha},t_{zb}}\delta_{t_{z\beta},t_{za}}]\\ =&\sum_{i<j}^A\sum_{t_{z\alpha},t_{z\beta}}[\delta_{t_{z\alpha},t_{za}}\delta_{t_{z\beta},t_{zb}}+(1-\delta_{t_{za},t_{zb}})\delta_{t_{z\alpha},t_{zb}}\delta_{t_{z\beta},t_{za}}],\end{aligned} \tag{21}$$

which is an integer equal to the number of pairs with a given pair of isospin projections (It is not an integer before summing over S). It will become more clear when we present the calculation results in Sec. IV A.

Considering all possible isospin projection pair configurations,

$$\begin{aligned}\langle r^0\rangle =&\sum_{t_{za}\le t_{zb}}\langle r^0[t_{za},t_{zb}]\rangle\\ =&\sum_{i<j}^{A}\sum_{t_{za}\le t_{zb}}\sum_{t_{z\alpha},t_{z\beta}}[\delta_{t_{z\alpha},t_{za}}\delta_{t_{z\beta},t_{zb}}+(1-\delta_{t_{za},t_{zb}})\\ &\times\delta_{t_{z\alpha},t_{zb}}\delta_{t_{z\beta},t_{za}}]\\ =&\sum_{i<j}^{A}1=\frac{A(A-1)}{2},\end{aligned}\tag{22}$$

which is the total number of nucleon pairs when evaluated within states of an A-nucleon system.

E. Square-separation operator

The expectation value of the square-separation operator r^2 in the two-body space describes the relative distance squared for a pair of nucleons. The square-separation operator for a fixed pair of isospin values and a fixed two-body total spin S can be defined as $\mathcal{O}(r)[S,t_{za},t_{zb}]=r^2[S,t_{za},t_{zb}]\equiv r^2P_SP_{t_{za},t_{zb}}$. Its expectation value in an A-body space

$$\langle r^2[S,t_{za},t_{zb}]\rangle=\sum_{\text{all q\#}}\sum_{i<j}^{A}{}_{ij}\langle\alpha\beta;J|r^2P_SP_{t_{za},t_{zb}}|\gamma\delta;J\rangle_{ij}.\tag{23}$$

We recall the relative mean-square-radius operator for a system of A nucleons [30, 31] (also called the mean-square intrinsic coordinate operator in Ref. [29])

$$r^2_{\rm rel}\equiv\frac{1}{A}\sum_{i}^{A}(\vec{r}_i-\vec{R}_{\rm cm})^2=\frac{1}{A^2}\sum_{i<j}^{A}(\vec{r}_i-\vec{r}_j)^2=\frac{1}{A^2}r^2_A,\tag{24}$$

where the center-of-mass coordinates $\vec{R}_{\rm cm}=(\sum_i^A\vec{r}_i)/A$. To calculate the point-proton/neutron rms radius, it is convenient to first consider the corresponding relative mean-square-radius operator in each isospin projection pair sector (pp, pn and nn) [32], $r^2_{{\rm rel},pp}\equiv r^2_A[1/2,1/2]/A^2$, $r^2_{{\rm rel},pn}\equiv r^2_A[1/2,-1/2]/A^2=r^2_A[-1/2,1/2]/A^2$ and $r^2_{{\rm rel},nn}\equiv r^2_A[-1/2,-1/2]/A^2$, where

$$\begin{aligned}r^2_A[t_{za},t_{zb}]=&\sum_{i<j}^{A}{}_{ij}\langle\alpha\beta;J|r^2|\gamma\delta;J\rangle_{ij}\delta_{t_{z\alpha},t_{z\gamma}}\delta_{t_{z\beta},t_{z\delta}}\\ &\times[\delta_{t_{z\alpha},t_{za}}\delta_{t_{z\beta},t_{zb}}+(1-\delta_{t_{za},t_{zb}})\delta_{t_{z\alpha},t_{zb}}\delta_{t_{z\beta},t_{za}}]\end{aligned}\tag{25}$$

is the square-separation operator projecting on a given isospin pair in an A-body space. The mean-square radius operators for protons and neutrons relative to the center-of-mass of all the nucleons are [30]

$$\begin{aligned}r^2_p\equiv&\frac{1}{Z}\sum_{i}^{A}\delta_{t_{zi},\frac{1}{2}}(\vec{r}_i-\vec{R}_{\rm cm})^2,\\ r^2_n\equiv&\frac{1}{N}\sum_{i}^{A}\delta_{t_{zi},-\frac{1}{2}}(\vec{r}_i-\vec{R}_{\rm cm})^2.\end{aligned}\tag{26}$$

It can be easily shown that [32]

$$\begin{aligned}r^2_p=&(2A/Z-1)r^2_{{\rm rel},pp}+(A/Z-1)r^2_{{\rm rel},pn}-r^2_{{\rm rel},nn},\\ r^2_n=&-r^2_{{\rm rel},pp}+(A/N-1)r^2_{{\rm rel},pn}+(2A/N-1)r^2_{{\rm rel},nn},\end{aligned}\tag{27}$$

where A, Z and N are the nucleon, proton and neutron numbers, respectively. Then the point-proton (neutron) rms radius r_p (r_n) can be calculated by taking the square root of the expectation value of r^2_p (r^2_n). The point-nucleon matter rms radius r_m can be calculated by taking the square root of the expectation value of $r^2_{\rm rel}$ (also denoted as r^2_m), or by utilizing the relation $Ar^2_m=Zr^2_p+Nr^2_n$.

III. *AB INITIO* NCSM CALCULATION USING MFDn

In the *ab initio* NCSM, we consider a system of point-like non-relativistic nucleons that interact by realistic inter-nucleon interactions. The two-nucleon or two-nucleon combining with three-nucleon interaction is taken from fitting two-nucleon phase shifts with high precision up to a certain energy and adjusting the remaining parameters of the three-nucleon interaction to a selection of three-nucleon observables. Although we do not employ the three-nucleon interactions explicitly [33–35], we plan to employ them in future studies that go beyond the scope of this work.

As the name NCSM implies, all the nucleons are considered active without an inert core that is assumed in standard, valence space, shell model calculations. The Hamiltonian operator for an A-nucleons system is thus

$$H_A=\sum_{i<j}^{A}\frac{(\vec{p}_i-\vec{p}_j)^2}{2m_{\rm N}A}+\sum_{i<j}^{A}V_{ij}+\sum_{i<j<k}^{A}V_{ijk}+...\tag{28}$$

where V_{ij} is the two-nucleon interaction, V_{ijk} is the three-nucleon interaction, and so on.

We solve the eigenvalue problem

$$H_A|\Phi_A\rangle=E|\Phi_A\rangle\tag{29}$$

in the harmonic-oscillator (HO) basis with energy spacing between shells $\hbar\Omega$ and many-body truncation $N_{\rm max}$ (the quanta of each shell is $2n+l$, where n and l are the radial and orbital angular momentum quantum numbers, respectively; $N_{\rm max}$ defines the maximum total number of quanta allowed in the many-body basis states for this

nucleus above the minimum required by the Pauli principle).

The calculations are carried out using MFDn (Many-Fermion Dynamics–nuclear), a configuration interaction (CI) code for nuclear structure calculations [36, 37]. It is a platform-independent Fortran 90 code using a hybrid MPI/OpenMP programming model, and is being used on current supercomputers, such as Cori and Perlmutter at NERSC, for *ab initio* calculations of atomic nuclei using realistic interactions.

We adopt the Daejeon16 two-nucleon (NN) interaction [38] in our *ab initio* NCSM calculations. This interaction is obtained by softening the chiral effective field theory (χEFT) generated Idaho next-to-next-to-next-to-leading order (N3LO) NN interaction using the similarity renormalization group (SRG) method [39, 40]. A special feature of this interaction is that it is an NN interaction that attempts to absorb the effects of interactions that might otherwise be treated as three and higher many-body forces, through phase-equivalent transformations (PETs) [41]. The optimal set of PET parameters are obtained by fitting the binding energies and spectra of selected light nuclei up to ^{16}O. The Daejeon16 interaction provides a good convergence rate in *ab initio* calculations for light nuclei compared with other realistic interactions [42, 43]. Ground state energies and radii calculated using this interaction are in reasonable agreement with the results of experiments for p-shell nuclei [44]. Recently, the applications of Daejeon16 have been extended to medium and heavy nuclei [45] using a mean-field with the inclusion of a phenomenological 3-body contact interaction. In addition, the Daejeon16 interaction has found many applications in scattering and resonances using the single-state HO representation of scattering equations (SS-HORSE) method [46–50].

The Daejeon16 interaction we use in this work has a maximum total angular momentum cut-off $J_{\max} = 6$. Because NN interactions are short-range and we are interested in only the ground states of these light nuclei, contributions from larger values of J to the expectation value of $\mathcal{O}(r)$ are anticipated to be vanishingly small. In addition, we superimpose the Coulomb interaction between protons onto the Daejeon16 NN interaction since the construction of Daejeon16 interaction is charge/isospin independent.

After obtaining the matrix elements of operators $O(r) = r^0$ and $O(r) = r^2$ in the HO basis (Appendix A), we then take the additional step to transform these matrix elements from the two-body relative frame to two-body matrix elements in the single-particle basis by the Moshinsky transformation sketched in Appendix B. The resulting two-body matrix elements are then employed to calculate expectation values using many-body NCSM wavefunctions.

To determine suitable parameters of many-nucleon basis space cutoff $N_{\max}$ and HO energy spacing in the *ab initio* NCSM calculation $\hbar\Omega$, we calculate r_p, r_n and r_m in a grid of $N_{\max}$ from 6 to 18 with a step size of 2, and $\hbar\Omega$ from 10 to 30 MeV with an increment of 2.5 MeV at a time. Two additional points at the lower end of $\hbar\Omega$ (8 and 9 MeV) are also calculated, to show the rapid growing trend at lower $\hbar\Omega$ (except $N_{\max} = 18$, for its relative flatter trend around $\hbar\Omega = 10$ MeV at $N_{\max} = 18$ compared with lower $N_{\max}$ and the higher computational cost associated with each point at $N_{\max} = 18$; more points will be calculated in future works when we perform an extrapolation, and we are currently satisfied with those points to give us an rough estimation of the uncertainty). The results are shown in Fig. 1. Using these results as a reference, we select $N_{\max} = 16$ and $\hbar\Omega = 10$ MeV for calculating the expectation values of the pair-identity operator and the square-separation operator, which will then be combined to give the mean square separation. $\hbar\Omega = 10$ to 27.5 MeV is found to provide an approximate $N_{\max}$ independence for the point-nucleon rms radii for ^{4}He, which can be seen in Fig. 2 through the almost invisible differences in the point-nucleon rms radii (Δr) between $N_{\max} = 16$ and $N_{\max} = 18$. For ^{6}He, the current calculations do not show a good convergence pattern. Meanwhile, Δr seems to decrease to 0 faster at lower $\hbar\Omega$, inferred by Δr between $N_{\max} = 14$ and $N_{\max} = 16$ (gray points). We choose $\hbar\Omega = 10$ to maintain an approximate convergence for ^{4}He while squeezing the differences of the point-nucleon rms radii values between neighboring $N_{\max}$ for ^{6}He. $N_{\max} = 16$ is chosen because it is sufficient for our demonstration goal and reasonable regarding the total computational resources needed. By comparing the rms radii for $\hbar\Omega = 10$ MeV from $N_{\max} = 18$ with those from $N_{\max} = 16$ (Fig. 2), we estimate that the error of point-nucleon rms radii due to basis truncation $N_{\max} = 16$ with $\hbar\Omega = 10$ MeV are $10^{-2} \sim 10^{-1}$ fm for ^{6}He and 10^{-3} fm for ^{4}He.

One interesting thing to note is that the $\hbar\Omega$ corresponding to the minimum difference of point-nucleon rms radius between $N_{\max} = 18$ and $N_{\max} = 16$ is not always identical across r_p, r_n and r_m. For example, in ^{4}He, the corresponding $\hbar\Omega = 15$ MeV for $r_{p/m}$ and 17.5 MeV for r_n. We also note that these $\hbar\Omega$ are generally smaller than the $\hbar\Omega$ for the minimum energy gap between $N_{\max} = 18$ and $N_{\max} = 16$. For instance, in ^{4}He, $\hbar\Omega = 17.5$ MeV at the minimum energy gap, slightly greater than the $\hbar\Omega$ at the minimum $r_{p/m}$ gap. In ^{6}He, $\hbar\Omega = 12.5$ MeV at the minimum energy gap is larger than the $\hbar\Omega$ at the minimum $r_{p/n/m}$ gap (less than 10 MeV). With the observation that the minimum energy gap for ^{4}He and ^{6}He moves towards a smaller $\hbar\Omega$ as basis size ($N_{\max}$) increases (Fig. 3), it seems that point-nucleon rms radii are more sensitive to the changing of basis size compared with the ground state energy.

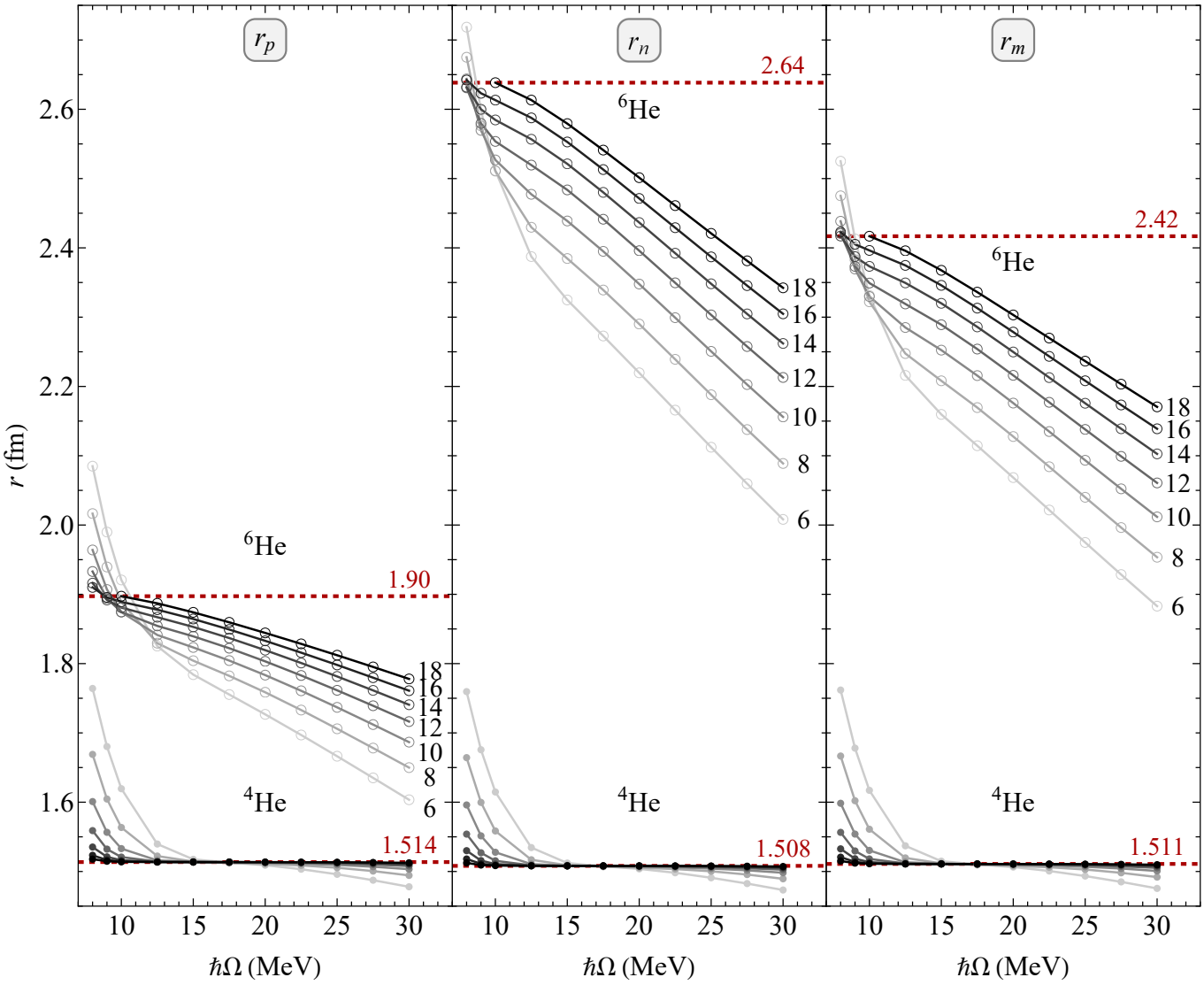

FIG. 1. r_p, r_n and r_m of ^{4}He and ^{6}He with Daejeon16 interaction plus Coulomb potential, calculated by MFDn for *ab initio* NCSM. Results for ^{4}He (^{6}He) are represented by filled (open) circles, which are connected by a sequence of straight lines for the same $N_{\max}$. The $N_{\max}$ values for ^{6}He are shown on the right of the sequences of lines, with increasing opacity as $N_{\max}$ increases. The horizontal dashed lines in each panel indicate the $r_{p/n/m}$ values of ^{4}He and ^{6}He for $N_{\max} = 18$ with $\hbar\Omega$ corresponding to the minimum gap between the calculated points for $N_{\max} = 18$ and $N_{\max} = 16$ (in ^{4}He, $\hbar\Omega = 15$ MeV for $r_{p/m}$ and $\hbar\Omega = 17.5$ MeV for r_n; in ^{6}He, $\hbar\Omega = 10$ MeV.).

IV. RESULTS AND ANALYSIS

A. The expectation value of pair-identity operator

The expectation value of a pair-identity operator $\langle r^0[S, t_{za}, t_{zb}]\rangle$ provides the probability of finding a pair of nucleons with fixed two-body total spin S and given isospin projections $\{t_{za}, t_{zb}\}$. The results of $\langle r^0[S, t_{za}, t_{zb}]\rangle$ for both values of S and for all the $\{t_{za}, t_{zb}\}$ combinations are presented in Table I.

Let us first perform a sanity check for the sum of $\langle r^0[S, t_{za}, t_{zb}]\rangle$ over all $\{S, t_{za}, t_{zb}\}$ combinations for ^{4}He and ^{6}He in the last row of Table I and confirm that they are equal to the total number of nucleon pairs $A(A-1)/2$ for each nucleus as indicated by Eq. (22). We note that although the calculated $\langle r^0[S, t_{za}, t_{zb}]\rangle$ are not integers, a sum of $\langle r^0[S, t_{za}, t_{zb}]\rangle$ over two-body total spin S equals to an integer number of pairs with given $\{t_{za}, t_{zb}\}$ in ^{4}He and ^{6}He, as suggested in Eq. (21). For example, both $\langle r^0[0, 1/2, 1/2]\rangle_{^4\mathrm{He}} = 0.976772$ and $\langle r^0[1, 1/2, 1/2]\rangle_{^4\mathrm{He}} = 0.023228$ are non-integers, while $\langle r^0[1/2, 1/2]\rangle_{^4\mathrm{He}} = 0.976772 + 0.023228 = 1.000000$, recovering an integer number (within 5 significant digits).

We expect and find that pp and nn in the ground state of ^{4}He are dominantly spin-singlet, because this is the only $l = 0$ basis state (s-state) respecting the overall anti-

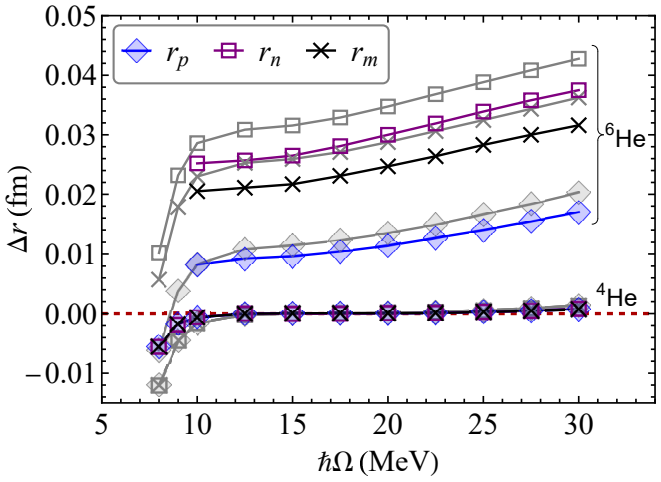

FIG. 2. Δr obtained by subtracting $r_{p/n/m}$ for $N_{\max} = 18$ ($N_{\max} = 16$) from those for $N_{\max} = 16$ ($N_{\max} = 14$), shown in color (gray) points. The absolute value $|\Delta r|$ serves as an indicator of the major source of the uncertainty of $r_{p/n/m}$ for ^{4}He and ^{6}He at $N_{\max} = 16$ in the *ab initio* NCSM calculation.

TABLE I. $\langle r^0[S, t_{za}, t_{zb}]\rangle$ for ^{4}He and ^{6}He with $N_{\max} = 16$ and $\hbar\Omega = 10$ MeV using the Daejeon16 interaction plus Coulomb potential, calculated by MFDn with an accuracy of 5 significant digits (denoted as "calc."). To display these numbers in a uniform format, 6 decimal digits are shown (digits after the significant digits are grayed out). The naively expected value (denoted as "naive") of each calculated result, based on occupying only the lowest available states in a HO basis, is listed for comparison as discussed in the text. The sum of each column is shown in the last line, which is equal to the number of pairs $A(A-1)/2$ for each nucleus.

		^{4}He		^{6}He	
	S	naive	calc.	naive	calc.
pp	0	1	0.976772	1	0.967578
pp	1	0	0.023228	0	0.032422
pn	0	1	0.979111	2	1.977430
pn	1	3	3.020890	6	6.022570
nn	0	1	0.976774	3	2.865420
nn	1	0	0.023226	3	3.134580
#pairs		6	6.000001	15	15.000000

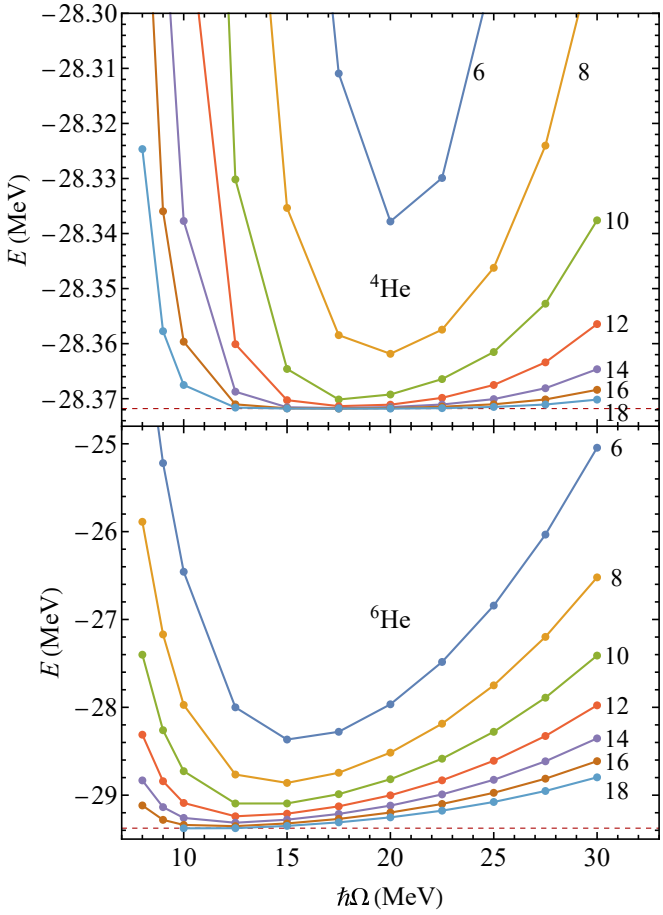

FIG. 3. The ground state energy with different $N_{\max}$ and $\hbar\Omega$ for ^{4}He and ^{6}He, using Daejeon16 interaction plus Coulomb potential, calculated by MFDn for *ab initio* NCSM. $N_{\max}$ is labeled alongside the sequence of lines connecting the values calculated for the same $N_{\max}$. The horizontal dashed lines indicate the ground state energy of ^{4}He and ^{6}He for $N_{\max} = 18$ with $\hbar\Omega$ corresponding to the minimum gap between the calculated points for $N_{\max} = 18$ and $N_{\max} = 16$. In ^{4}He, $\hbar\Omega = 17.5$ MeV; in ^{6}He, $\hbar\Omega = 12.5$ MeV.

symmetrization for exchanging of two isospin-symmetric fermions, i.e. $(-1)^{l+S+T} = -1$, where l, S and T are the two-body total orbital angular momentum in the two-body relative frame (See Appendix B), two-body total spin and two-body total isospin, respectively. One may also expect, as we indeed find, a small but non-zero portion of triplet (0.023228 for $\{pp, S = 1\}$ and 0.023226 for $\{nn, S = 1\}$) arising from partial wave contributions at higher values of l. The added Coulomb potential makes the isospin symmetry only approximate in our calculations (note that we assume equal mass for the p and the n which is taken as the average mass of these nucleons and Daejeon16 is charge-independent), which will contribute to the difference of expectation values between pp and nn pairs for ^{4}He. However, this deviation should be small and consistent with the fact that isospin is known to be a very good symmetry for light nuclei, as revealed in the approximately balanced pp and nn results for ^{4}He in Table I.

For the spin-independent parts of the NN interactions, singlet and triplet two-body spin states have the same energy in the same HO wave function of relative motion (labeled by n and l for two-body central potentials)—there is no preference among the allowed two-body spin configurations $\uparrow\uparrow$ (triplet), $\downarrow\downarrow$ (triplet), $\uparrow\downarrow + \downarrow\uparrow$ (triplet) and $\uparrow\downarrow - \downarrow\uparrow$ (singlet). As a result, the ratio of the probability of triplet to singlet two-body spin states for the ground state of ^{4}He pn pairs is approximately 3:1. Upon

considering the spin-dependent part of the NN potential, e.g. S_pS_n coupling in the s-state, which can be usefully written as $V_{\rm spin} = \hbar^{-2}V_1(r)\vec{S}_p\cdot\vec{S}_n$ [51], the probability of finding an pn pair in one of the triplet states can be slightly larger than in the singlet state if $V_1(r)$ is effectively attractive (thus negative), as in deuterium. This assessment takes into account that $\langle\vec{S}_p\cdot\vec{S}_n\rangle = +\hbar^2/4$ for triplet states and $-3\hbar^2/4$ for singlet states. These expectations are met, as can be seen in the calculated pn results of ^{4}He in Table I.

We then inspect $\langle r^0[S,t_{za},t_{zb}]\rangle$ of ^{6}He in Table I. To pave the way for later discussions, we digress a bit to highlight the difference between ^{4}He and ^{6}He when their constituent nucleons occupy the lowest possible single-particle states of a HO basis. Unlike ^{4}He, at the ground state of ^{6}He, there are two additional neutrons that are unable to occupy the lowest single-particle state due to the Pauli exclusion principle. This can be immediately seen from the ground state proton and neutron occupation probabilities (Fig. 4). For ^{4}He, the two lowest s-states ($0s_{1/2}$ and $1s_{1/2}$) contribute about 90% of the total occupation number, which is 2 for either protons or neutrons. For ^{6}He, these two states still contribute about 1.74/2=87% of the proton number, but only gather about 1.83/4=46% of the neutron number. On the other hand, the occupancy of neutrons at $0p_{1/2}$ ($0p_{3/2}$) is 0.22 (1.70), which contributes 5% (43%) of the neutron number. This suggests that, in ^{6}He, two neutrons largely remain in the lowest two single-particle s-states (mainly $0s_{1/2}$, with 1.73 occupancy)—regarded as the "α core" neutrons, and the other two neutrons are mainly in the $0p_{3/2}$ state—regarded as the valence neutrons.

Following the analyses above, it turns out that the calculated $\langle r^0[S,t_{za},t_{zb}]\rangle$ of ^{6}He in Table I are consistent with the naive expectations described below, with a maximum deviation of 0.14, which is small on these scales. pp should largely stay at the singlet state, inferred by the moderate change of proton occupancy from ^{4}He to ^{6}He (Fig. 4). The two "α core" neutrons of ^{6}He shall correlate similarly as the ^{4}He neutrons do with the protons. In other words, it is thrice as likely to find a triplet state than to find a singlet state in the pn pairs within the "α core". Among the eight pn pairs of ^{6}He, the ratio of triplet states to singlet states in the other four pn pairs might be the same as the "α core" pn pairs. The reason is as follows. Since for ^{6}He neutrons, $0s_{1/2}$ and $0p_{3/2}$ states are approximately equal in contribution, while the rest of states are highly suppressed, we can consider the "α core" neutrons and the valence neutrons as two groups only differing by unperturbed orbitals occupied. Therefore, when neutrons in each group form two-body total spin with the protons, ideally, there should be again no preference among the four two-body total spin states, $\uparrow\uparrow$ (triplet), $\downarrow\downarrow$ (triplet), $\uparrow\downarrow+\downarrow\uparrow$ (triplet) and $\uparrow\downarrow-\downarrow\uparrow$ (singlet). In addition, the two protons can be regarded as the third group with the same nucleon occupancy. The two-body total spin states in nn pairs formed by inter-group neutrons (one n comes from the "α core" and the other n comes from the valence shell) shall mimic the ones in pn pairs. Multiplying the total number pairs by the probability of taking each two-body total spin state, we expect three nn pairs in triplet states and one nn pair in singlet states, for nn pairs formed by inter-group neutrons. To a lesser extent, we shall also expect to have another two nn pairs in singlet states, one formed by the two "α core" neutrons and the other formed by the two valence neutrons, assuming the correlations of neutrons within each shell are more important than correlations of neutrons across different shells. This assumption shall be mostly true, because the difference between the expected and calculated $\langle r^0[S,t_{za},t_{zb}]\rangle$ for ^{6}He nn pairs in Table I is only 0.14, which is small on these scales.

It is interesting to note that when we exclude the ^{6}He nn pairs in our consideration, the largest deviation between the calculated results and their naively expected integer values is only 0.033 for ^{6}He and 0.024 for ^{4}He. This is consistent with our speculation that the two valence neutrons have an insignificant influence on the "α core" two-body total spin configurations. Fig. 5 is a possible arrangement of the spin and orbital angular momentum of the two valence neutrons of ^{6}He speculated from Fig. 4(b), for the ground state dominant configuration satisfying $\vec{S}=\vec{s}_1+\vec{s}_2=0$, where $\vec{s}_1$ and $\vec{s}_2$ are the spin of the two valence neutrons. It should be noted that the real picture for the orbital rotation is more complicated, because at least the center-of-mass motion should be supplemented to this simplified picture. As a consequence, for the ground state with $l=0$, the orbital angular momentum of the two valence neutrons ($\vec{l}_1$ and $\vec{l}_2$) are not necessarily antiparallel, i.e., $\vec{l}_1$ and $\vec{l}_2$ contain information of the residual center-of-mass motion.

We now address the role of $N_{\rm max}$ truncation. The maximum difference of $\langle r^0[S,t_{za},t_{zb}]\rangle$ between $N_{\rm max}=16$ and $N_{\rm max}=14$ is 1×10^{-4} for ^{6}He pp/pn pairs and 5×10^{-4} for ^{6}He nn pairs. Keeping in mind that the MFDn calculation preserves 5 significant digits, it is meaningful that the dependence on basis truncation still resides in the 4th decimal digit of the results. On the other hand, for ^{4}He, the maximum difference of $\langle r^0[S,t_{za},t_{zb}]\rangle$ between $N_{\rm max}=16$ and $N_{\rm max}=14$ is 4×10^{-5}, so the uncertainty due to truncation that we quote only appears in the 5th decimal digit.

To investigate which two-body states dominate in $\langle r^0\rangle$, we examine the major two-body states (labeled by spectroscopic notation $n\,^{2S+1}l_J$, where $|l-S|\le J\le|l+S|$) of $\langle r^0\rangle$ for the three isospin-projected pair configurations, shown in Fig. 6. For ^{4}He ground state, all the major components come from s-states, as naively expected from the shell model. ^{4}He pp is mostly (81%) at the lowest singlet state, with a small portion (12%) at the $n=1$ singlet s-state. ^{6}He pp is almost identical to ^{4}He. ^{4}He pn triplet states are dominated by the lowest two s-states (96%), while ^{4}He pn singlet is dominated by the lowest s-state (81%). For ^{6}He pn pairs, we see the rising of p/d-states in both singlet and triplet configurations. The three major p-states contribute 22% and the $0\,^3d_3$ state contributes

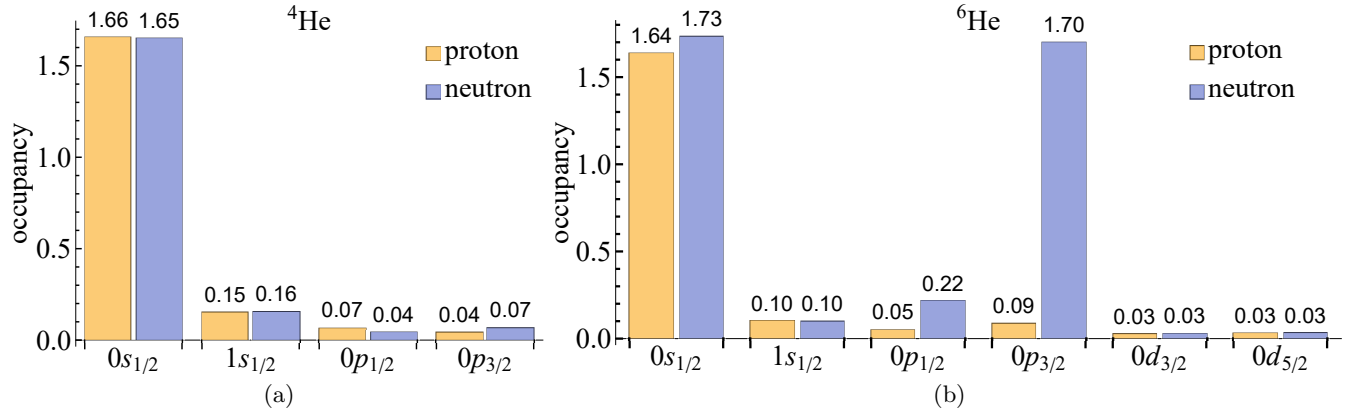

FIG. 4. Occupancy of protons or neutrons on single-particle states for the ground state ^{4}He (a) and ^{6}He (b), with $N_{\max} = 16$ and $\hbar\Omega = 10$ MeV. The single-particle states that are major contributors are shown, which collectively contribute more than 90% of the proton number or neutron number of each nucleus.

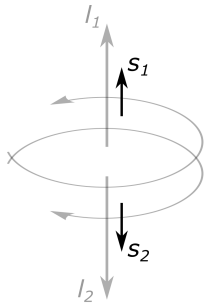

FIG. 5. The sketch of a possible arrangement for the the spin and orbital angular momentum of the two valence neutrons of ^{6}He in the ground state dominant configuration.

1% of $\langle r^0 \rangle$. For nn, we again see the rising of higher states (45% p-states and 2% $0\,^1d_2$) in ^{6}He. We note that, for nn, due to the $(-1)^{l+S+T} = -1$ antisymmetry constraint, all allowed p-states are triplets and all allowed s/d-states are singlets. It follows that, ^{6}He nn triplets are dominantly at p-states and ^{6}He nn singlets are dominantly at s-states.

To sum up, we conclude that the two ^{6}He valence neutrons dominantly form a singlet spin configuration and mostly in s-states, from the consideration of preserving ^{4}He two-body total spin configuration inside ^{6}He (suggested by the fact that the proton/neutron occupation probabilities at $0s_{1/2}$ single particle state in Fig. 4 and pp two-body spin states in Fig. 6(a) remain almost unchanged from ^{4}He to ^{6}He), and from the fairly good consistency between the *ab initio* NCSM calculated $\langle r^0 \rangle$ and the naively expected values (Table I). This provides an indicator of halo structure in ^{6}He through the following reasoning. The nn singlet s-states have symmetrical spatial wave functions Ψ_{nlm} which have non-zero probability close to the center-of-mass of the pair due to the absence of a centrifugal term in the relative Schrödinger equation, resulting in a stronger correlation between the two nucleons compared with triplet states. This seems to support a "di-neutron" halo at some distance from the center-of-mass of the nucleus. The "cigar"-like configuration is another possibility seen in many calculations but appears not to be the dominant configuration [1, 52, 53].

It can be seen from the above analyses that the *ab initio* NCSM calculated $\langle r^0 \rangle$ is useful for speculating the structure of the ground state ^{6}He. These analyses are quantitatively limited by the symmetry assumptions involved. We assume the ^{4}He two-body total spin configuration is preserved inside ^{6}He. We further assume the equal probabilities of taking the four possible two-body spin configurations ($\uparrow\uparrow$, $\downarrow\downarrow$, $\uparrow\downarrow + \downarrow\uparrow$, $\uparrow\downarrow - \downarrow\uparrow$) for pn or nn pairs that are "indistinguishable", where "indistinguishable" between two nucleon pairs means that each p or n in one nucleon pair comes from the same group as a p or n in the other nucleon pair, and vice versa (one-to-one correspondence). As mentioned above, there are three groups of nucleons in ^{6}He, "α core" neutrons, valence neutrons and protons. To mitigate the impact of these assumptions, we quantitatively investigate the single-particle state occupation probabilities and the major two-body spectroscopic components of $\langle r^0 \rangle$ in this section. Another route brings in the results of the other operators for relaxing these symmetry constraints as demonstrated in the coming section Sec. IV B.

B. The expectation value of square-separation operator

The expectation values of the square-separation operator for different two-body total spin and isospin projections $\langle r^2[S, t_{za}, t_{zb}] \rangle$ are presented in Table II. To normalize $\langle r^2[S, t_{za}, t_{zb}] \rangle$ to its average value for a single pair of nucleons, we define the mean square separation between two nucleons of given $\{S, t_{za}, t_{zb}\}$ as

$$\overline{\langle r^2[S, t_{za}, t_{zb}] \rangle} \equiv \frac{\langle r^2[S, t_{za}, t_{zb}] \rangle}{\langle r^0[S, t_{za}, t_{zb}] \rangle}, \tag{30}$$

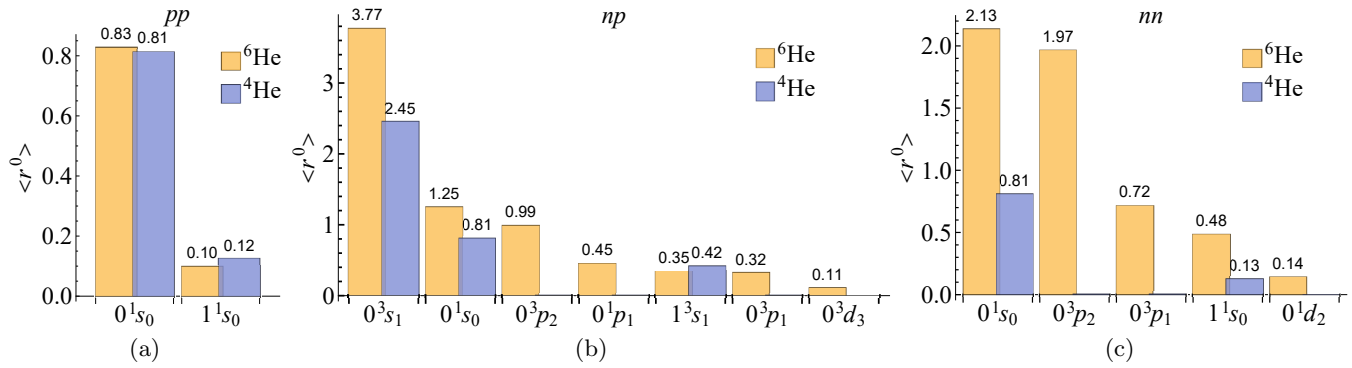

FIG. 6. Major $\langle r^0 \rangle$ two-body contributions of the ground state ^{4}He and ^{6}He with $N_{\max} = 16$ and $\hbar\Omega = 10$ MeV, for pp (a), pn (b) and nn (c) pair configurations. The bins are arranged in decreasing order for ^{6}He, with the corresponding ^{4}He bins shown alongside for comparison. The above shown states in total contribute more than 90% of $\langle r^0 \rangle$ in each isospin-projected pair configuration.

and the rms separation between two nucleons of given $\{S, t_{za}, t_{zb}\}$

$$\overline{\langle r^2[S,t_{za},t_{zb}]\rangle}^{1/2} \equiv \sqrt{\frac{\langle r^2[S,t_{za},t_{zb}]\rangle}{\langle r^0[S,t_{za},t_{zb}]\rangle}}. \quad (31)$$

These derived quantities are shown in the last two columns for each nucleus in Table II.

TABLE II. $\langle r^2[S,t_{za},t_{zb}]\rangle$ [fm^2] for ^{4}He and ^{6}He with $N_{\max} = 16$ and $\hbar\Omega = 10$ MeV using the Daejeon16 interaction plus Coulomb potential, calculated by MFDn with an accuracy of 5 significant digits (digits after the significant digits are grayed out). We also present in the second (third) column of each nucleus the mean square separation $\overline{\langle r^2[S,t_{za},t_{zb}]\rangle}$ [fm^2] (the rms separation $\overline{\langle r^2[S,t_{za},t_{zb}]\rangle}^{1/2}$ [fm]). The last line shows the sum of $\langle r^2[S,t_{za},t_{zb}]\rangle$ for each nucleus.

		^{4}He			^{6}He		
	S	$\langle r^2\rangle$	$\overline{\langle r^2\rangle}$	$\overline{\langle r^2\rangle}^{1/2}$	$\langle r^2\rangle$	$\overline{\langle r^2\rangle}$	$\overline{\langle r^2\rangle}^{1/2}$
pp	0	5.95862	6.10032	2.46988	6.63201	6.85424	2.61806
pp	1	0.22754	9.79581	3.12983	0.36145	11.1484	3.33892
pn	0	5.94563	6.07248	2.46424	24.5046	12.3921	3.52024
pn	1	18.3172	6.06352	2.46242	73.2384	12.1607	3.48721
nn	0	5.89396	6.03411	2.45644	38.7177	13.5121	3.67588
nn	1	0.22648	9.75110	3.12268	63.2643	20.1827	4.49252
sum		36.5695	-	-	206.718	-	-

These results can be interpreted with the following considerations. Using again the overall antisymmetrization property of fermion pairs as mentioned in Sec. IV A, the rms separation for singlet is expected to be smaller than triplet for the pp and nn pairs in their lowest partial waves. This turns out to be true for both ^{4}He (2.5 fm versus 3.1 fm) and ^{6}He (2.6 fm versus 3.3 fm for pp; 3.7 fm versus 4.5 fm for nn) seen in Table II. For pn pairs, since the total two-body isospin T can be either 0 or 1, the spatial part of the wave function for given S can be either symmetric or antisymmetric. Thus, the rms separation for singlet pn pairs and triplet pn pairs are similar (2.46 fm for both in ^{4}He; 3.52 fm and 3.49 fm, in ^{6}He).

Comparing ^{6}He with ^{4}He, we see that the rms separation for pp singlet configuration, which is the dominant two-body spin configuration of pp, is expanded by 6% from ^{4}He to ^{6}He. Interestingly, the remaining $\sim$3% (Table I) portion pp triplet states also experiences a similar expansion in rms separation from ^{4}He to ^{6}He, even though they are negligible. On the other hand, the rms separation for nn and pn pairs are expanded by 40%$\sim$50% from ^{4}He to ^{6}He.

Summing over S in both denominator and numerator of Eq. (30), we define the mean square separation for nucleon pairs of given $\{t_{za}, t_{zb}\}$ as

$$\overline{\langle r^2[t_{za},t_{zb}]\rangle} \equiv \frac{\sum_S \langle r^2[S,t_{za},t_{zb}]\rangle}{\sum_S \langle r^0[S,t_{za},t_{zb}]\rangle} = \frac{\langle r^2[t_{za},t_{zb}]\rangle}{\langle r^0[t_{za},t_{zb}]\rangle}. \quad (32)$$

^{4}He and ^{6}He has only one pp, $\langle r^0[1/2,1/2]\rangle_{^4\mathrm{He},^6\mathrm{He}} = 1$. Similarly, it is straightforward to note that $\langle r^0[-1/2,1/2]\rangle_{^4\mathrm{He}} = 4$, $\langle r^0[-1/2,1/2]\rangle_{^6\mathrm{He}} = 8$, $\langle r^0[-1/2,-1/2]\rangle_{^4\mathrm{He}} = 1$ and $\langle r^0[-1/2,-1/2]\rangle_{^6\mathrm{He}} = 6$. The rms separation of given $\{t_{za}, t_{zb}\}$ can be defined as the square root of the above quantity. The calculated mean square separations along with the rms separations are shown in Table III, consistent with the corresponding results computed using NNLO$_{\mathrm{opt}}$ nucleon-nucleon interaction [54] with $N_{\max} = 14$ in Ref. [55] (^{4}He $\overline{\langle r^2\rangle}_{pp}^{1/2} \approx$ 2.40 fm; ^{6}He $\overline{\langle r^2\rangle}_{pp}^{1/2} \approx$ 2.62 fm, $\overline{\langle r^2\rangle}_{pn}^{1/2} \approx$ 3.3 fm and $\overline{\langle r^2\rangle}_{pp}^{1/2} \approx$ 3.9 fm).

To describe a nucleus by nucleon-nucleon separation without specifying nucleon species, we define the mean square separation between two nucleons in a nucleus

$$\overline{\langle r^2\rangle} \equiv \frac{\sum_{S,t_{za}\le t_{zb}} \langle r^2[S,t_{za},t_{zb}]\rangle}{\sum_{S,t_{za}\le t_{zb}} \langle r^0[S,t_{za},t_{zb}]\rangle} = \frac{\langle r^2\rangle}{A(A-1)/2}, \quad (33)$$

TABLE III. $\langle r^2[t_{za},t_{zb}]\rangle$ [fm^2] computed from Table II, together with the mean square separation $\overline{\langle r^2[t_{za},t_{zb}]\rangle}$ [fm^2] and the rms separation $\overline{\langle r^2[t_{za},t_{zb}]\rangle}^{1/2}$ [fm]. Digits after the 5 significant digits are grayed out.

	^{4}He			^{6}He		
	$\langle r^2\rangle$	$\overline{\langle r^2\rangle}$	$\overline{\langle r^2\rangle}^{1/2}$	$\langle r^2\rangle$	$\overline{\langle r^2\rangle}$	$\overline{\langle r^2\rangle}^{1/2}$
pp	6.18616	6.18616	2.48720	6.99346	6.99346	2.64452
pn	24.2629	6.06572	2.46287	97.7429	12.2179	3.49541
nn	6.12044	6.12044	2.47395	101.982	16.9970	4.12274

where $A(A-1)/2=6$ for ^{4}He and $A(A-1)/2=15$ for ^{6}He. Then the rms nucleon-nucleon separation within a nucleus is the square root of $\overline{\langle r^2\rangle}$. From Table II and Eq. (33), $\overline{\langle r^2\rangle}_{^4\mathrm{He}}=6.0949$ fm^2 and $\overline{\langle r^2\rangle}_{^6\mathrm{He}}=13.781$ fm^2, which yield $\overline{\langle r^2\rangle}^{1/2}_{^4\mathrm{He}}=2.4688$ fm and $\overline{\langle r^2\rangle}^{1/2}_{^6\mathrm{He}}=3.7123$ fm, meaning that the nucleon-nucleon separations of ^{6}He, on average, are 50% larger than those of ^{4}He.

One way to estimate the "halo" effect of ^{6}He is to compare the neutron radius of ^{6}He with ^{4}He. One can make use of the calculated binding energy of ^{4}He and ^{6}He ($N_{\max}=16$, $\hbar\omega=10$ MeV), which are -28.3597 MeV and -29.3387 MeV, respectively. Subtracting these two values gives two-neutron separation energy for ^{6}He $\Delta E_s=0.979$ MeV. From the characteristic wave number $k_{\mathrm{ch}}=\sqrt{m_N\Delta E_s/\hbar^2}\sim0.15$ fm^{-1}, the corresponding neutron radius is $\sim$6.5 fm. Similarly, for ^{4}He, $k_{\mathrm{ch}}\sim0.7$ fm^{-1} can be obtained by additional *ab initio* NCSM calculations of ground state binding energy, e.g., -7.75 MeV for ^{3}He (-8.44 MeV for ^{3}H) with $N_{\max}=22$ and $\hbar\omega=10(12.5)$ MeV (the ground state energy is nearly convergent at these $N_{\max}$ and $\hbar\omega$ values). Thus, the neutron and proton radius of ^{4}He is about 1.4 fm. The discrepancy between the estimated neutron radius of ^{6}He and ^{4}He could signal the formation of a "halo" in ^{6}He. However, the characteristic wave number is based on s-states. As shown in Fig. 6, p/d-states also play an important role in nn and pn pairs of ^{6}He.

To make a more quantitative estimation of the "halo" effect of ^{6}He, we compute and present in Table IV r_p, r_n and r_m for ^{4}He and ^{6}He, by combining the calculated $\langle r^2[t_{za},t_{zb}]\rangle$ with Eq. (27), with $N_{\max}=16$ and $\hbar\Omega=10$. r_p^*, r_n^* and r_m^* are the ones obtained with $N_{\max}=18$ and $\hbar\Omega$ corresponding to the minimum gap Δr between $N_{\max}=18$ and $N_{\max}=16$ (indicated in Fig. 1). Comparing $r_{p/n/m}$ and $r^*_{p/n/m}$ gives an estimation of the magnitude of the basis cut-off uncertainties. For ^{4}He, the differences appear in the third decimal digit. For ^{6}He, the differences show up in the second decimal digit.

The experimental point-nucleon rms radii are indicated in the last column of each nucleus in Table IV. The point-proton rms radius is calculated using $r_p^2=r_c^2-R_p^2-3/(4M_p^2)-(N/Z)R_n^2-r_{so}^2$, where the nucleus rms charge radius r_c can be measured from laser spectroscopy or scattering experiments, the Darwin-Foldy term $3/(4M_p^2)=0.033$ fm^2 [56] and the neutron mean square charge radius $R_n^2=-0.1161(22)$ [56]. The relativistic correction due to spin-orbit interaction $r_{so}^2=0$ for ^{4}He and -0.08 fm^2 for ^{6}He [57]. Considering the discrepancy between two groups of experimental proton charge radius after an experiment using muonic hydrogen atoms [58] (see Refs. [59, 60] for recent reviews), we present results calculated by two values of proton mean square charge radius, $R_p^2=0.7658(93)$ (CODATA 2016 [61]) and $R_p^2=0.7071(6)$ (PDG 2020 [56]), separated by a slash. The experimental range of r_m in Table IV is obtained from interaction cross sections of elastic scattering [62]. The experimental r_n is computed from the relation $Ar_m^2=Zr_p^2+Nr_n^2$. The point-nucleon rms radii are relatively well-converged for ^{4}He but the desired fully convergent point-nucleon rms radii for ^{6}He have not been achieved with this limited basis size. The calculation results are in reasonable agreement with the experimental values within the uncertainty ranges. The calculated ^{4}He r_p is slightly larger than the experimental values by 0.02$\sim$0.06 fm, with a moderate decreasing trend as basis size increases. The calculated ^{6}He r_p is slightly smaller (by 0.01$\sim$0.07 fm) than the experimental values while increasing as the basis size increases.

From Table IV, the calculated point-proton and point-neutron rms radii for ^{4}He are nearly identical, around $r_0=1.51$ fm. And from Table III, ^{4}He pp, pn and nn rms separations are also very similar, about $a=2.47$ fm. The ratio $a/r_0=1.636$ is approximately the same as the side length to the center-to-vertex distance ratio of a tetrahedron $2\sqrt{6}/3=1.633$. This suggests a route by which we can relate our quantum many-body results to a classical picture that depicts ^{4}He as a tetrahedron with protons and neutrons at the tetrahedron's vertices.

In Table III, the pp rms separation of ^{6}He increases by 6.3%, while the pn (nn) rms separation of ^{6}He increases by 41.9% (66.6%), compared with those of ^{4}He. It turns out that the main feature of these changes can be captured by a binary model. We introduce x (y) as the ratio between the rms separation of pn or nn consisting only of the "α core" nucleons (contains at least one nucleon outside the "α core") in ^{6}He and the rms separation of pn or nn in ^{4}He, i.e.,

$$\frac{r^{(^6\mathrm{He})}_{pn/nn,i}}{r^{(^4\mathrm{He})}_{pn/nn}}=\begin{cases} x, & \text{both nucleons within the "}\alpha\text{ core"}\\ y, & \text{otherwise}\end{cases}. \tag{34}$$

Matching the percentage increases,

$$\frac{r^{(^6\mathrm{He})}_{pn}-r^{(^4\mathrm{He})}_{pn}}{r^{(^4\mathrm{He})}_{pn}}=\sqrt{\frac{4x^2+4y^2}{8}}-1=41.9\%, \tag{35}$$

and

$$\frac{r^{(^6\mathrm{He})}_{nn}-r^{(^4\mathrm{He})}_{nn}}{r^{(^4\mathrm{He})}_{nn}}=\sqrt{\frac{x^2+5y^2}{6}}-1=66.6\%. \tag{36}$$

TABLE IV. The expectation value of $r^2_{p/n/m}$ [fm^2] and $r_{p/n/m}$ [fm] for ^{4}He and ^{6}He, calculated by *ab initio* NCSM with $\hbar\Omega = 10$ MeV and $N_{\max} = 16$ using Daejeon16 plus Coulomb interaction. Digits after the 5 significant digits are grayed out. $r^*_{p/n/m}$ [fm] is the rms radius for $N_{\max} = 18$, with $\hbar\Omega$ corresponding to the minimum gap Δr between $N_{\max} = 18$ and $N_{\max} = 16$ (Fig. 1), served as a reference for the uncertainty owning to the $N_{\max}$ truncation. The experimental values are shown in the last column of each nucleus, where r_p and r_m are separately measurable, and the experimental r_n is obtained using $Ar^2_m = Zr^2_p + Nr^2_n$.

	^{4}He				^{6}He			
x	r^2_x	r_x	r^*_x	r_x(exp.)	r^2_x	r_x	r^*_x	r_x(exp.)
p	2.29381	1.51453	1.5136	1.464(6)/1.484(5) [63]	3.56864	1.88908	1.8973	1.938(23)/1.953(22) [64]
n	2.27738	1.50910	1.5081	1.43–1.84	6.82895	2.61323	2.6384	2.35–3.08
m	2.28559	1.51182	1.5109	1.46–1.66 [62]	5.74218	2.39628	2.4168	2.23–2.75 [62]

Solving these two equations yields $x = 0.93$ and $y = 1.78$. This suggests that the pn/nn rms separation for the "α core" stays nearly the same as for ^{4}He, while the rms separation of pn/nn not belonging to the "α core" is found to increase by almost 80%, indicating the formation of a halo.

It should be noted that the simple binary model treats the "α core" as approximately a point mass when viewed by each of the two valence neutrons, ignoring the fact that the size of the "α core" is comparable to the distance between the valence neutrons and the core. In fact, similar pictures are often adopted in current *ab initio* calculations where clustering information is input as a piece of prior knowledge.

Finally, we observe that the point-proton rms radius increases by 25% from ^{4}He ($r_p = 1.515$ fm) to ^{6}He ($r_p = 1.889$ fm) (Table IV). This increase may be understood as the consequence of a halo structure, arising from the motion of the charged "α core" around the common center-of-mass as well as possible contributions from swelling of the "α core" [62].

V. CONCLUSION AND ADDITIONAL DISCUSSIONS

We show that the formation of the halo structure of ^{6}He can be examined from the coordinate-space two-body correlation operators. More specifically, we analyze the *ab initio* NCSM calculation results of the pair-identity operator (r^0) and the square-separation operator (r^2) for different nucleon pairs with fixed two-body total spin and two-body total angular momentum. We illustrate the dominant two-body spin configurations of ^{4}He and ^{6}He by analyzing the results of r^0. We demonstrate that the inclusion of r^2 provides a more subtle picture of ^{6}He, by utilizing the calculated point-nucleon rms radius and a binary model constructed using the calculated rms separations between nucleons.

We believe that the spatial correlation operators can refine our understanding of halo nuclei, beyond the general application of using them to calculate the point-nucleon rms radius r_p, r_n and r_m. This paper demonstrates the usefulness of r^0 and r^2 in analyzing the nuclear structure. We are also interested in exploring other spatial correlation operators, such as r^4 and r^6, to see what additional information is available. In addition, we speculate there may be a systematic way to combine those spatial correlation results to provide a richer physical picture of the structure of light nuclei.

There is a need to develop robust extrapolation techniques for spatial correlation operators that are long-range and difficult to converge with increasing the basis size ($N_{\max}$). Even though both ^{4}He and ^{6}He ground state energy seems to saturate around the $\hbar\Omega$ corresponding to the variational minimum (Fig. 3), their point-nucleon rms radii present a more complicated pattern (Fig. 1). Ref. [65] proposed a two-dimensional twisted tape extrapolation using point-nucleon radii results from *ab initio* NCSM with Daejeon16 interaction plus Coulomb interaction for ^{6}He (the largest basis for ^{6}He adopted in this paper is the one with $N_{\max} = 14$). The finite $N_{\max}$ point-nucleon rms radii for ^{4}He in this paper are identical to ours, but the ones for ^{6}He in this paper are slightly ($\sim$0.01 MeV) smaller than ours. The extrapolated point-nucleon rms radii in Ref. [65] for ^{6}He are $r_p = 1.871(16)$ fm, $r_n = 2.663(3)$ fm and $r_m = 2.430(6)$ fm. This r_p is slightly smaller than our r_p for $N_{\max} = 16$ and $N_{\max} = 18$ (Table IV), which might partially result from their slightly smaller r_p in finite basis. The extrapolated r_n and r_m in Ref. [65] are larger than the values we obtained for $N_{\max} = 16$ and $N_{\max} = 18$ (Table IV). Since our r_n and r_m have an increasing trend with increasing $N_{\max}$ around the region with the least $\hbar\Omega$ dependence, it appears reasonable that we would obtain a higher value of $r_{n/m}$ after extrapolation.

We view this work as the first step in a series of efforts we intend to make to reveal the spatial structure of exotic nuclei using *ab initio* calculation results. Since our nuclear structure studies are non-relativistic, one may foresee *ab initio* calculations that fuel driven semi-classical models capable of presenting detailed structural information of a nucleus with intuitive appeal. We will illustrate this in our future works.

ACKNOWLEDGMENTS

This work was supported in part by the US Department of Energy (DOE) under Grant Nos. DE-FG02-87ER40371, DE-SC0018223 (SciDAC-4/NUCLEI), DE-SC0023495 (SciDAC-5/NUCLEI) and DE-SC0023707 (Quantum Horizons – NuHaQ). It was performed under the auspices of the U.S. Department of Energy by Lawrence Livermore National Laboratory under Contract DE-AC52-07NA27344. Computational resources were provided by the National Energy Research Scientific Computing Center (NERSC), which is supported by the US DOE Office of Science under Contract No. DE-AC02-05CH11231. Tobias Frederico thanks the hospitality of the Department of Physics and Astronomy of the Iowa State University and to the Fulbright Brazil for the financial support during his visits on 2018 and 2019. TF also thanks CNPq grant 308486/2015-3, INCT-FNA project 464898/2014-5 and FAPESP Thematic grants 2017/05660-0 and 2019/07767-1. Peng Yin is supported by the Strategic Priority Research Program of Chinese Academy of Sciences, Grant No. XDB34000000. The ND nuclear theory grant number is DE-FG02-95ER40934.

Appendix A: Harmonic oscillator matrix elements

One can obtain the matrix elements of operators $O(r) = r^0$ and $O(r) = r^2$ in the convenient HO basis with the knowledge that the angular parts of the wavefunctions are not affected, so only matrix elements with $l = l'$ are non-zero:

$$\langle n'l'|r^0|nl\rangle = \delta_{n,n'}\delta_{l,l'}, \tag{A1}$$

$$\begin{aligned}&\langle n'l'|r^2|nl\rangle\\ &= b^2\left[(2n+l+\frac{3}{2})\delta_{n,n'} - \sqrt{n(n+l+\frac{1}{2})}\delta_{n,n'+1}\right.\\ &\left.-\sqrt{(n+1)(n+l+\frac{3}{2})}\delta_{n,n'-1}\right]\delta_{l,l'},\end{aligned} \tag{A2}$$

where $b \equiv \sqrt{\hbar/(\mu\Omega)}$ with the reduced mass $\mu = m_{\rm N}/2$ ($m_{\rm N} = 938.92$ MeV/c^2 is the average mass of a neutron and a proton with their mass given by PDG [56]) representing the reduced mass of a nucleon in the two-body subsystem. The derivation of these matrix elements has been detailed in the Appendix of Ref. [66].

Appendix B: Moshinsky transformation

We follow the Moshinsky transformation as discussed in Ref. [67]. The single particle HO wave functions in the two-body relative frame are

$$\langle\vec{r}|nlm\rangle. \tag{B1}$$

The two-body oscillator wave function with total angular momentum L and its projection λ reads

$$\begin{aligned}&\langle\vec{r}_1\vec{r}_2|n_1l_1n_2l_2L\lambda\rangle\\ &=R_{n_1l_1}(r_1)R_{n_2l_2}(r_2)\sum_{m_1m_2}C^{\,l_1\ l_2\ L}_{m_1m_2\lambda}Y_{l_1m_1}(\mathbf{\Omega}_1)Y_{l_2m_2}(\mathbf{\Omega}_2).\end{aligned} \tag{B2}$$

Noting that the two-body relative coordinates

$$\vec{r} = \frac{1}{\sqrt{2}}(\vec{r}_1 - \vec{r}_2), \quad \vec{R} = \frac{1}{\sqrt{2}}(\vec{r}_1 + \vec{r}_2), \tag{B3}$$

and introducing the two-body center-of-mass orbital angular momentum $\mathcal{L}$ and its projection $\mathcal{M}$, and the center-of-mass radial quantum number $\mathcal{N}$, one arrives at

$$\begin{aligned}\langle\vec{r}\vec{R}|n_1l_1n_2l_2L\lambda\rangle &= \sum_{l\mathcal{L}}\psi_i(r,R)\\ &\times\sum_{m\mathcal{M}}C^{\,l\ \ \mathcal{L}\ L}_{m\ \mathcal{M}\lambda}\,Y_{lm}(\mathbf{\Omega}_r)Y_{\mathcal{L}\mathcal{M}}(\mathbf{\Omega}_R),\end{aligned} \tag{B4}$$

where $i \equiv \{n_1l_1n_2l_2l\mathcal{L}L\}$, and

$$\psi_i(r,R) = \sum_{n\mathcal{N}}(nl,\mathcal{N}\mathcal{L};L|n_1l_1,n_2l_2;L)_1R_{nl}(r)R_{\mathcal{N}\mathcal{L}}(R), \tag{B5}$$

with the well-known Moshinsky brackets $(nl,\mathcal{N}\mathcal{L};L|n_1l_1,n_2l_2;L)_1$ subscripted by the ratio of the mass of the two bodies (see e.g. Ref. [68]).

[1] M. V. Zhukov, B. V. Danilin, D. V. Fedorov, J. M. Bang, I. J. Thompson, and J. S. Vaagen, Bound state properties of Borromean halo nuclei: ^{6}He and ^{11}Li, Physics Reports **231**, 151 (1993).

[2] P. G. Hansen, A. S. Jensen, and B. Jonson, Nuclear halos, Annual review of nuclear and particle science **45**, 591 (1995).

[3] A. S. Jensen, K. Riisager, D. V. Fedorov, and E. Garrido, Structure and reactions of quantum halos, Rev. Mod. Phys. **76**, 215 (2004).

[4] B. Jonson, Light dripline nuclei, AIP Conference Proceedings **495**, 3 (1999).

[5] K. Riisager, Halos and related structures, Physica Scripta **T152**, 014001 (2013).

[6] I. Tanihata, H. Hamagaki, O. Hashimoto, Y. Shida, N. Yoshikawa, K. Sugimoto, O. Yamakawa, T. Kobayashi, and N. Takahashi, Measurements of interaction cross sections and nuclear radii in the light

p-shell region, Phys. Rev. Lett. **55**, 2676 (1985).

[7] I. Tanihata, Neutron halo nuclei, Journal of Physics G: Nuclear and Particle Physics **22**, 157 (1996).

[8] I. Tanihata, Nuclear physics with RIB's: How it all started, The European Physical Journal Plus **131**, 90 (2016).

[9] T. Kobayashi, O. Yamakawa, K. Omata, K. Sugimoto, T. Shimoda, N. Takahashi, and I. Tanihata, Projectile fragmentation of the extremely neutron-rich nucleus ^{11}Li at 0.79 GeV/nucleon, Phys. Rev. Lett. **60**, 2599 (1988).

[10] N. A. Orr, N. Anantaraman, S. M. Austin, C. A. Bertulani, K. Hanold, J. H. Kelley, D. J. Morrissey, B. M. Sherrill, G. A. Souliotis, M. Thoennessen, J. S. Winfield, and J. A. Winger, Momentum distributions of ^{9}Li fragments following the breakup of ^{11}Li, Phys. Rev. Lett. **69**, 2050 (1992).

[11] T. Nakamura, A. M. Vinodkumar, T. Sugimoto, N. Aoi, H. Baba, D. Bazin, N. Fukuda, T. Gomi, H. Hasegawa, N. Imai, M. Ishihara, T. Kobayashi, Y. Kondo, T. Kubo, M. Miura, T. Motobayashi, H. Otsu, A. Saito, H. Sakurai, S. Shimoura, K. Watanabe, Y. X. Watanabe, T. Yakushiji, Y. Yanagisawa, and K. Yoneda, Observation of strong low-lying $E1$ strength in the two-neutron halo nucleus ^{11}Li, Phys. Rev. Lett. **96**, 252502 (2006).

[12] T. Aumann, D. Aleksandrov, L. Axelsson, T. Baumann, M. J. G. Borge, L. V. Chulkov, J. Cub, W. Dostal, B. Eberlein, T. W. Elze, H. Emling, H. Geissel, V. Z. Goldberg, M. Golovkov, A. Grünschloß, M. Hellström, K. Hencken, J. Holeczek, R. Holzmann, B. Jonson, A. A. Korshenninikov, J. V. Kratz, G. Kraus, R. Kulessa, Y. Leifels, A. Leistenschneider, T. Leth, I. Mukha, G. Münzenberg, F. Nickel, T. Nilsson, G. Nyman, B. Petersen, M. Pfützner, A. Richter, K. Riisager, C. Scheidenberger, G. Schrieder, W. Schwab, H. Simon, M. H. Smedberg, M. Steiner, J. Stroth, A. Surowiec, T. Suzuki, O. Tengblad, and M. V. Zhukov, Continuum excitations in ^{6}He, Phys. Rev. C **59**, 1252 (1999).

[13] N. Fukuda, T. Nakamura, N. Aoi, N. Imai, M. Ishihara, T. Kobayashi, H. Iwasaki, T. Kubo, A. Mengoni, M. Notani, H. Otsu, H. Sakurai, S. Shimoura, T. Teranishi, Y. X. Watanabe, and K. Yoneda, Coulomb and nuclear breakup of a halo nucleus ^{11}Be, Phys. Rev. C **70**, 054606 (2004).

[14] C. Romero-Redondo, P. Navrátil, S. Quaglioni, and G. Hupin, *Ab initio* NCSM/RGM for three-body cluster systems and application to $^{4}\mathrm{He} + n + n$, Few-Body Systems **55**, 927 (2014).

[15] S. Quaglioni, P. Navrátil, G. Hupin, J. Langhammer, C. Romero-Redondo, and R. Roth, No-core shell model analysis of light nuclei, Few-Body Systems **54**, 877 (2013).

[16] C. Romero-Redondo, S. Quaglioni, P. Navrátil, and G. Hupin, $^{4}\mathrm{He} + n + n$ continuum within an *ab initio* framework, Phys. Rev. Lett. **113**, 032503 (2014).

[17] P. Navrátil, Cluster form factor calculation in the *ab initio* no-core shell model, Phys. Rev. C **70**, 054324 (2004).

[18] S. Quaglioni, C. Romero-Redondo, P. Navrátil, and G. Hupin, Three-cluster dynamics within the *ab initio* no-core shell model with continuum: How many-body correlations and α clustering shape ^{6}He, Phys. Rev. C **97**, 034332 (2018).

[19] E. Epelbaum, H. Krebs, T. A. Lähde, D. Lee, and U.-G. Meißner, Structure and rotations of the Hoyle state, Phys. Rev. Lett. **109**, 252501 (2012).

[20] T. Otsuka, T. Abe, T. Yoshida, Y. Tsunoda, N. Shimizu, N. Itagaki, Y. Utsuno, J. Vary, P. Maris, and H. Ueno, α-Clustering in atomic nuclei from first principles with statistical learning and the Hoyle state character, Nature Communications **13**, 2234 (2022).

[21] C. Robin, M. J. Savage, and N. Pillet, Entanglement rearrangement in self-consistent nuclear structure calculations, Phys. Rev. C **103**, 034325 (2021).

[22] B. R. Barrett, P. Navrátil, and J. P. Vary, *Ab initio* no core shell model, Progress in Particle and Nuclear Physics **69**, 131 (2013).

[23] C. Cockrell, J. P. Vary, and P. Maris, Lithium isotopes within the *ab initio* no-core full configuration approach, Phys. Rev. C **86**, 034325 (2012).

[24] C. Cockrell, *Ab initio nuclear structure calculations for light nuclei (2012)*, Ph.D. thesis, Iowa State University (2012).

[25] J. W. Negele, *Quantum many-particle systems* (CRC Press, 2018).

[26] A. R. Edmonds, *Angular Momentum in Quantum Mechanics* (Princeton University Press, 2016).

[27] D. M. Brink and G. R. Satchler, *Angular momentum* (Oxford University Press, USA, 1968).

[28] E. U. Condon, E. U. Condon, and G. H. Shortley, *The theory of atomic spectra* (Cambridge University Press, 1951).

[29] M. A. Caprio, A. E. McCoy, and P. J. Fasano, Intrinsic operators for the translationally-invariant many-body problem, Journal of Physics G: Nuclear and Particle Physics **47**, 122001 (2020).

[30] S. Bacca, N. Barnea, and A. Schwenk, Matter and charge radius of ^{6}He in the hyperspherical-harmonics approach, Phys. Rev. C **86**, 034321 (2012).

[31] M. A. Caprio, P. Maris, and J. P. Vary, Coulomb-Sturmian basis for the nuclear many-body problem, Phys. Rev. C **86**, 034312 (2012).

[32] M. A. Caprio, P. Maris, and J. P. Vary, Halo nuclei ^{6}He and ^{8}He with the Coulomb-Sturmian basis, Phys. Rev. C **90**, 034305 (2014).

[33] J. Carlson, V. Pandharipande, and R. Wiringa, Three-nucleon interaction in 3-, 4- and ∞-body systems, Nuclear Physics A **401**, 59 (1983).

[34] S. C. Pieper, V. R. Pandharipande, R. B. Wiringa, and J. Carlson, Realistic models of pion-exchange three-nucleon interactions, Phys. Rev. C **64**, 014001 (2001).

[35] S. Coon, M. Scadron, P. McNamee, B. Barrett, D. Blatt, and B. McKellar, The two-pion-exchange three-nucleon potential and nuclear matter, Nuclear Physics A **317**, 242 (1979).

[36] P. Maris, M. Sosonkina, J. P. Vary, E. Ng, and C. Yang, Scaling of ab-initio nuclear physics calculations on multi-core computer architectures, Procedia Computer Science (ICCS 2010) **1**, 97 (2010).

[37] H. M. Aktulga, C. Yang, E. G. Ng, P. Maris, and J. P. Vary, Improving the scalability of a symmetric iterative eigensolver for multi-core platforms, Concurrency and Computation: Practice and Experience **26**, 2631 (2014).

[38] A. Shirokov, I. Shin, Y. Kim, M. Sosonkina, P. Maris, and J. Vary, N3LO NN interaction adjusted to light nuclei in *ab exitu* approach, Physics Letters B **761**, 87 (2016).

[39] F. Wegner, Flow-equations for Hamiltonians, Annalen der Physik **506**, 77 (1994).

[40] S. D. Glazek and K. G. Wilson, Perturbative renormalization group for Hamiltonians, Phys. Rev. D **49**, 4214

(1994).
[41] W. N. Polyzou and W. Glöckle, Three-body interactions and on-shell equivalent two-body interactions, Few-Body Systems **9**, 97 (1990).
[42] I. J. Shin, *Ab initio* calculations for Li isotopes with Daejeon16, in *Proceedings of the Ito International Research Center Symposium "Perspectives of the Physics of Nuclear Structure"*.
[43] Y. Kim, I. J. Shin, A. M. Shirokov, M. Sosonkina, P. Maris, and J. P. Vary, Daejeon16 *NN* interaction, arXiv:1910.04367 [nucl-th] (2019).
[44] P. Maris, I. J. Shin, and J. P. Vary, *Ab initio* structure of *p*-shell nuclei with chiral effective field theory and Daejeon16 interactions, arXiv:1908.00155 [nucl-th] (2019).
[45] P. Papakonstantinou, J. P. Vary, and Y. Kim, Daejeon16 interaction with contact-term corrections for heavy nuclear systems, J. Phys. G **48**, 085105 (2021).
[46] A. M. Shirokov, A. I. Mazur, I. A. Mazur, E. A. Mazur, I. J. Shin, Y. Kim, L. D. Blokhintsev, and J. P. Vary, Nucleon-α scattering and resonances in ^{5}He and ^{5}Li with JISP16 and Daejeon16 *NN* interactions, Phys. Rev. C **98**, 044624 (2018).
[47] A. I. Mazur, A. M. Shirokov, I. A. Mazur, L. D. Blokhintsev, Y. Kim, I. J. Shin, and J. P. Vary, Description of continuum states within the no-core shell model: Single-state HORSE method, Physics of Atomic Nuclei **82**, 537 (2019).
[48] I. A. Mazur, A. M. Shirokov, A. I. Mazur, I. J. Shin, Y. Kim, P. Maris, and J. P. Vary, Description of continuum spectrum states of light nuclei in the shell model, Physics of Particles and Nuclei **50**, 537 (2019).
[49] A. M. Shirokov, Y. Kim, A. I. Mazur, I. A. Mazur, I. J. Shin, and J. P. Vary, Tetraneutron resonance: Theory, AIP Conference Proceedings **2038**, 020038 (2018).
[50] I. A. Mazur, I. J. Shin, Y. Kim, A. I. Mazur, A. M. Shirokov, P. Maris, and J. P. Vary, SS-HORSE extension of the no-core shell model: Application to resonances in ^{7}He, Phys. Rev. C **106**, 064320 (2022).
[51] P. Cappellaro, Chapter 5. Nuclear Structure, in *22.02 Introduction to Applied Nuclear Physics. Spring 2012* (MIT OpenCourseWare. License: Creative Commons BY-NC-SA. Massachusetts Institute of Technology, Cambridge, MA, 2012).
[52] K. Hagino and H. Sagawa, Pairing correlations in nuclei on the neutron-drip line, Phys. Rev. C **72**, 044321 (2005).
[53] G. Papadimitriou, A. T. Kruppa, N. Michel, W. Nazarewicz, M. Płoszajczak, and J. Rotureau, Charge radii and neutron correlations in helium halo nuclei, Phys. Rev. C **84**, 051304 (2011).
[54] A. Ekström, G. Baardsen, C. Forssén, G. Hagen, M. Hjorth-Jensen, G. R. Jansen, R. Machleidt, W. Nazarewicz, T. Papenbrock, J. Sarich, and S. M. Wild, Optimized chiral nucleon-nucleon interaction at next-to-next-to-leading order, Phys. Rev. Lett. **110**, 192502 (2013).
[55] D. Sääf, *Bridging scales in nuclear physics*, Ph.D. thesis (2016).
[56] P. A. Zyla et al. (Particle Data Group), Prog. Theor. Exp. Phys. 2020 , 083C01 (2020).
[57] A. Ong, J. C. Berengut, and V. V. Flambaum, Effect of spin-orbit nuclear charge density corrections due to the anomalous magnetic moment on halonuclei, Phys. Rev. C **82**, 014320 (2010).
[58] R. Pohl, A. Antognini, F. Nez, F. D. Amaro, F. Biraben, J. M. R. Cardoso, D. S. Covita, A. Dax, S. Dhawan, L. M. P. Fernandes, A. Giesen, T. Graf, T. W. Hänsch, P. Indelicato, L. Julien, C.-Y. Kao, P. Knowles, E.-O. Le Bigot, Y.-W. Liu, J. A. M. Lopes, L. Ludhova, C. M. B. Monteiro, F. Mulhauser, T. Nebel, P. Rabinowitz, J. M. F. dos Santos, L. A. Schaller, K. Schuhmann, C. Schwob, D. Taqqu, J. F. C. A. Veloso, and F. Kottmann, The size of the proton, Nature **466**, 213 (2010).
[59] M. Tanabashi, K. Hagiwara, K. Hikasa, K. Nakamura, Y. Sumino, F. Takahashi, J. Tanaka, K. Agashe, G. Aielli, C. Amsler, M. Antonelli, D. M. Asner, H. Baer, S. Banerjee, R. M. Barnett, T. Basaglia, C. W. Bauer, J. J. Beatty, V. I. Belousov, J. Beringer, S. Bethke, A. Bettini, H. Bichsel, O. Biebel, K. M. Black, E. Blucher, O. Buchmuller, V. Burkert, M. A. Bychkov, R. N. Cahn, M. Carena, A. Ceccucci, A. Cerri, D. Chakraborty, M.-C. Chen, R. S. Chivukula, G. Cowan, O. Dahl, G. D'Ambrosio, T. Damour, D. de Florian, A. de Gouvêa, T. DeGrand, P. de Jong, G. Dissertori, B. A. Dobrescu, M. D'Onofrio, M. Doser, M. Drees, H. K. Dreiner, D. A. Dwyer, P. Eerola, S. Eidelman, J. Ellis, J. Erler, V. V. Ezhela, W. Fetscher, B. D. Fields, R. Firestone, B. Foster, A. Freitas, H. Gallagher, L. Garren, H.-J. Gerber, G. Gerbier, T. Gershon, Y. Gershtein, T. Gherghetta, A. A. Godizov, M. Goodman, C. Grab, A. V. Gritsan, C. Grojean, D. E. Groom, M. Grünewald, A. Gurtu, T. Gutsche, H. E. Haber, C. Hanhart, S. Hashimoto, Y. Hayato, K. G. Hayes, A. Hebecker, S. Heinemeyer, B. Heltsley, J. J. Hernández-Rey, J. Hisano, A. Höcker, J. Holder, A. Holtkamp, T. Hyodo, K. D. Irwin, K. F. Johnson, M. Kado, M. Karliner, U. F. Katz, S. R. Klein, E. Klempt, R. V. Kowalewski, F. Krauss, M. Kreps, B. Krusche, Y. V. Kuyanov, Y. Kwon, O. Lahav, J. Laiho, J. Lesgourgues, A. Liddle, Z. Ligeti, C.-J. Lin, C. Lippmann, T. M. Liss, L. Littenberg, K. S. Lugovsky, S. B. Lugovsky, A. Lusiani, Y. Makida, F. Maltoni, T. Mannel, A. V. Manohar, W. J. Marciano, A. D. Martin, A. Masoni, J. Matthews, U.-G. Meißner, D. Milstead, R. E. Mitchell, K. Mönig, P. Molaro, F. Moortgat, M. Moskovic, H. Murayama, M. Narain, P. Nason, S. Navas, M. Neubert, P. Nevski, Y. Nir, K. A. Olive, S. Pagan Griso, J. Parsons, C. Patrignani, J. A. Peacock, M. Pennington, S. T. Petcov, V. A. Petrov, E. Pianori, A. Piepke, A. Pomarol, A. Quadt, J. Rademacker, G. Raffelt, B. N. Ratcliff, P. Richardson, A. Ringwald, S. Roesler, S. Rolli, A. Romaniouk, L. J. Rosenberg, J. L. Rosner, G. Rybka, R. A. Ryutin, C. T. Sachrajda, Y. Sakai, G. P. Salam, S. Sarkar, F. Sauli, O. Schneider, K. Scholberg, A. J. Schwartz, D. Scott, V. Sharma, S. R. Sharpe, T. Shutt, M. Silari, T. Sjöstrand, P. Skands, T. Skwarnicki, J. G. Smith, G. F. Smoot, S. Spanier, H. Spieler, C. Spiering, A. Stahl, S. L. Stone, T. Sumiyoshi, M. J. Syphers, K. Terashi, J. Terning, U. Thoma, R. S. Thorne, L. Tiator, M. Titov, N. P. Tkachenko, N. A. Törnqvist, D. R. Tovey, G. Valencia, R. Van de Water, N. Varelas, G. Venanzoni, L. Verde, M. G. Vincter, P. Vogel, A. Vogt, S. P. Wakely, W. Walkowiak, C. W. Walter, D. Wands, D. R. Ward, M. O. Wascko, G. Weiglein, D. H. Weinberg, E. J. Weinberg, M. White, L. R. Wiencke, S. Willocq, C. G. Wohl, J. Womersley, C. L. Woody, R. L. Workman, W.-M. Yao, G. P. Zeller, O. V. Zenin, R.-Y. Zhu, S.-L. Zhu, F. Zimmermann, P. A. Zyla, J. Anderson, L. Fuller, V. S.

Lugovsky, and P. Schaffner (Particle Data Group), Review of particle physics, Phys. Rev. D **98**, 030001 (2018).
[60] H. Gao and M. Vanderhaeghen, The proton charge radius, Rev. Mod. Phys. **94**, 015002 (2022).
[61] P. J. Mohr, D. B. Newell, and B. N. Taylor, Codata recommended values of the fundamental physical constants: 2014, Journal of Physical and Chemical Reference Data **45**, 043102 (2016).
[62] Z.-T. Lu, P. Mueller, G. W. F. Drake, W. Nörtershäuser, S. C. Pieper, and Z.-C. Yan, Colloquium: Laser probing of neutron-rich nuclei in light atoms, Rev. Mod. Phys. **85**, 1383 (2013).
[63] I. Sick, Precise root-mean-square radius of ^{4}He, Phys. Rev. C **77**, 041302 (2008).
[64] M. Brodeur, T. Brunner, C. Champagne, S. Ettenauer, M. J. Smith, A. Lapierre, R. Ringle, V. L. Ryjkov, S. Bacca, P. Delheij, G. W. F. Drake, D. Lunney, A. Schwenk, and J. Dilling, First direct mass measurement of the two-neutron halo nucleus ^{6}He and improved mass for the four-neutron halo ^{8}He, Phys. Rev. Lett. **108**, 052504 (2012).
[65] D. M. Rodkin and Y. M. Tchuvil'sky, Two-dimensional extrapolation procedure for an ab initio study of nuclear size parameters and the properties of the halo nucleus ^{6}He, Phys. Rev. C **106**, 034305 (2022).
[66] R. A. M. Basili, *Nuclear properties with effective operators (2019)*, Ph.D. thesis, Iowa State University (2019).
[67] M. Znojil, Moshinsky brackets for light nuclei, Phys. Rev. C **15**, 423 (1977).
[68] M. Sotona and M. Gmitro, Generalized transformation brackets for the harmonic oscillator functions, Computer Physics Communications **3**, 53 (1972).